文章编号 2095-1531(2020)06-1362-23

# Absorption enhancement of silicon via localized surface plasmons resonance in blue band

WANG Hao-bing[1,2], TAO Jin[1], LV Jin-guang[1], MENG De-jia[1], LI Yang[1,2], ZHAO Yong-zhou[1,2], WANG Jia-xian[1,2], ZHANG Jun[3], QIN Yu-xin[1], WANG Wei-biao[1*], LIANG Jing-qiu[1*]

(1. *State Key Laboratory of Applied Optics*, *Changchun Institute of Optics*, *Fine Mechanics and Physics*, *Chinese Academy of Sciences*, *Changchun* 130033, *China*;
2. *University of Chinese Academy of Sciences*, *Beijing* 100049, *China*;
3. *Guangzhou Key Laboratory of Visible Light Communication Engineering Technology*, *Jinan University*, *Guangzhou* 510632, *China*)

* *Corresponding author*, *E-mail*: *wangwb@ciomp.ac.cn*; *liangjq@ciomp.ac.cn*

**Abstract**: To enhance the blue light absorption of silicon, an array of silver nanoparticles(Ag-NPs) was designed so that they create Localized Surface Plasmon Resonance(LSPR) near the surface of silicon(Si). The properties of the enhanced optical absorption of silicon in the blue band were then observed and researched. The blue-light absorption characteristic of silicon in the Ag-NPs/Silicon composite structure were calculated using the Finite-Difference-Time-Domain (FDTD) method. The results indicated that the metallic nanoparticles' extinction capability was related to its geometric parameters and the resonance intensity and peak wavelength can be tuned according to different geometric parameters of Ag-NPs including radius, height and period. At a resonance peak wavelength of 465 nm, the optical absorption of Si in the composite structure (Ag-NPs/Si) rises from 59% to 94% with an array of radius $r$ = 18.5 nm, a height $H$ = 45.0 nm and a period $P$ = 49.0 nm. It concluded that the light absorption gain was 0.57 and photogenerated carriers had a gain factor of 0.53 due to the enhanced light absorption of Si via LSPR in blue band. The results provide a significant reference for the enhancement of the blue-light absorption properties in silicon based on the LSPR effect and the design of a silicon-photodetector with a visible wide spectral resoponse.

**Key words**: localized surface plasmon; silicon; blue light; absorptivity; FDTD method

**收稿日期**:2020-04-02; **修订日期**:2020-04-27

**基金项目**:国家重点研发计划(批准号:2018YFB1801900)资助的课题,广东省科技计划项目 (批准号:2016B010111003) 资助的课题,吉林省科技发展计划项目 (批准号:20180801024GX 和 20190302062GX) 资助的课题,中国科学院青年创新促进会基金(批准号:2018254),应用光学国家重点实验室 2019 年度开放基金(SKLAO:201908)

Supported by the National Key Research and Development Program of China (Grant No. 2018YFB1801900), Science and Technology Plan of Guangdong Province, China (Grant No. 2016B010111003) and Development of Science and Technology Plan of Jilin Province, China (Grant No. 20180801024GX and No. 20190302062GX), the Youth Innovation Promotion Association Foundation (NO. 2018254), the State Key Laboratory of Applied Optics 2019 Open Foundation (SKLAO: 201908)

# 局域表面等离激元共振增强硅蓝光波段吸收特性研究

王浩冰[1,2], 陶　金[1], 吕金光[1], 孟德佳[1], 李　阳[1,2], 赵永周[1,2], 王家先[1,2],
张　军[3], 秦余欣[1], 王惟彪[1*], 梁静秋[1*]
（1. 中国科学院长春光学精密机械与物理研究所，应用光学国家重点实验室，长春 130033；
2. 中国科学院大学，北京 100049；
3. 暨南大学，广州市可见光通信工程技术重点实验室，广州 510632）

**摘要:** 为增强硅的蓝光吸收, 在硅表面设计银纳米颗粒阵列, 基于局域表面等离激元共振效应对增强的硅蓝光吸收特性进行了分析研究。采用有限时域差分法计算银纳米颗粒阵列/硅复合结构中硅的蓝光吸收特性。结果表明: 金属颗粒的消光能力与其几何参数有关, 改变银纳米颗粒阵列的半径 $r$、高度 $H$ 与周期 $P$ 可调控局域表面等离激元共振强度与共振频率, 当银纳米颗粒阵列参数设定为: $r$ = 18.5 nm、$H$ = 45 nm、$P$ = 49 nm 时, 在共振吸收波长为 465 nm 的情况下, 硅的蓝光吸收率由 59% 增加至 94%, 光吸收增益为 0.57, 光生载流子数目增益为 0.53, 分析认为是局域表面等离激元共振增强硅在蓝光波段的光吸收导致上述增益现象。本文的研究结果对了解局域表面等离激元效应, 改善硅的蓝光吸收特性, 设计和制备高蓝光响应度硅基可见光光电探测器具有重要的参考价值。

**关　键　词:** 局域表面等离激元; 硅; 蓝光; 吸收率; 有限时域差分法
**中图分类号:** O431.1; O436.2; O471.5　　**文献标志码:** A　　**doi:** 10.37188/CO.2020-0056

## 1　Introduction

In recent years, with the continuous development of Surface Plasmon (SP) theory and the continuous improvement of micro-nano processing technique, the sensitization of photoelectric detectors based on SPs[1] has aroused great interest among researchers. The SPs can increase the intensity of local electromagnetic field, enhance the interaction between light and matter[2], achieve selective light absorption and with an ultra-high absorption rate[3]. Thus their application in solar cells[4], LED[5-6], surface-enhanced Raman spectrum[7], photoelectric detection[8] and other fields has attracted extensive attention.

The material properties, geometric shape, structural parameters, medium background and other factors of micro-nano array will have an impact on the physical phenomena of SPs[9]. The nature of the material itself determines the main attenuation path of SPs so that the SPs will sensitize the photodetectors in different ways[10]. For example, in the event of Surface Plasmons Resonance (SPR) attenuation, the Au-Nanoparticles (Au-NPs) transfer the absorbed light energy to free electrons in the metal through Landau damping. Then the free electrons are converted into hot electrons, which jump over the Schottky barrier into the semiconductor to improve the optical response in the incident band. The attenuation pattern of SPR in the Ag-Nanoparticles (Ag-NPs) and Aluminum-Nanoparticles (Al-NPs) is to scatter the incident light energy to the medium through optical radiation[11], thus improving the light absorptivity of metal particle substrates and enhancing the photoelectric performance of photodetectors.

In 2011, Naomi Halas 's research group[12] demonstrated that Au-nanorods could realize thermoelectron detection with incident photon energy lower than silicon bandgap width $E_g$, and increase the photocurrent by a factor of 20 ($\lambda_{in}$ = 1.4 μm). In

2012, Li's research group[13] studied the photoelectric response performance of surface plasmon effect coupled with GaN-based detector. By preparing the Ag nanoparticles with non-uniform sizes on the GaN surface, the device responsiveness was improved by a factor of 30 ($\lambda_{in}$ = 0.36 μm). In 2013, Sobhani *et al*.[14] prepared the Au grating on Si surface. The silica-based thermoelectron detector based on Extraordinary Optical Transmission (EOT) effect had an optical response of 0.6 mA/W ($\lambda_{in}$ = 1.46 μm) with an internal quantum efficiency of 0.2%. In 2014, Bao *et al*.[15] studied the photoelectric performance gain of AlGaN-based solar blinded UV detector based on the Al-NPs with a non-uniform density. The performance of AlGaN detector was enhanced by exciting the surface plasmons, and its optical responser was increased from 0.144 A/W to 0.288 A/W ($\lambda_{in}$ = 0.288 μm). The above research shows that on the one hand, the excited SP effect of metal micro-nano structure can increase the probability that the incident photons are captured by detector to generate the hole-electron pair and photocurrent; on the other hand, based on the thermoelectronic effect, the efficiency of photocurrent generation can be significantly improved by crossing the Schottky barrier, thus effectively enhancing the working performance of a photodetector in the response band.

In silicon (Si), the excited carriers have a wide spectral response in the incident band of 380~1 100 nm. However, due to the relatively large absorption coefficient and small penetration depth of Si in the blue band, the photo-generated carriers can diffuse to the interface or surface state easily[16]. As a result, fewer photo-generated carriers diffuse and drift to the depletion region, leading to low quantum efficiency and optical response of silicon photodetector (Si-PD) in this band. However, efficient Si-based blue light detectors have a great potential application market in visible light communication[17], underwater communication[18], local intelligent positioning[19] and other fields.

So far, few reports have been made on the use of SPs to enhance the photoelectric performance of Si-PD in the blue band. In this paper, an array of metal nanoparticles was designed on the silicon surface. The Finite-Difference-Time-Domain (FDTD)[20] method was used to study the influence of metal nanoparticles with different geometric parameters on the light absorption characteristic of Si. The results were analyzed according to the physical properties of Localized Surface Plasmons (LSPs)[9]. The research on the influence of SPs on the blue light absorption of Si is expected to improve the blue light absorption of Si, so as to provide reference for the design and preparation of a Si-PD with high blue light detection efficiency based on SP enhancement.

## 2 Theoretical model

### 2.1 Localized Surface Plasmon (LSP) and FDTD numerical algorithm

If the size of metal particles is much smaller than the penetration depth of incident field, free electrons will oscillate relative to the metal lattice under the joint action of coulomb field and external electromagnetic field, and the generated non-propagating mixed excited state will be LSP[9], as shown in Fig.1.

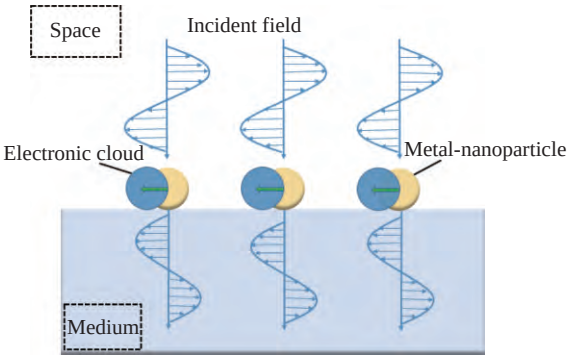


Fig. 1 Schematic diagram of localized surface plasmons with a metallic spherical structure

图 1 金属球状结构的局域表面等离激元示意图

Take metal spherical nanoparticles with a diameter of <100 nm as an example. Under the quasi-static approximation, the polarizability $\alpha$ can be

used to describe the interaction between incident light and particles and represent the LSP intensity. Its expression is

$$\alpha = 4\pi a^3 \left( \frac{\varepsilon - \varepsilon_m}{\varepsilon + 2\varepsilon_m} \right), \quad (1)$$

where $a$ is the particle radius; $\varepsilon_m$ is the relative dielectric constant of the background environment; and $\varepsilon$ is the relative complex dielectric constant of a metal particle, which is affected by the frequency of incident electromagnetic field, the characteristics and size of material, and other factors. According to the Eq. (1), when $\mathrm{Re}[\varepsilon] = -2\varepsilon_m$, the polarizability $\alpha$ is the maximum and the Localized Surface Plasmons Resonance (LSPR) is excited. $\mathrm{Re}[\varepsilon] = -2\varepsilon_m$ is also called Fröhlich condition[9]. When the metal nanoparticles are in the LSPR state, the polarizability and the efficiency of incident light absorption and scattering are the maximum. Generally, the extinction cross section $\sigma_{\mathrm{ext}}$ represents its total optical response with a numerical relationship of $\sigma_{\mathrm{ext}} = \sigma_{\mathrm{abs}} + \sigma_{\mathrm{scat}}$, where $\sigma_{\mathrm{abs}}$ and $\sigma_{\mathrm{scat}}$ are the optical absorption cross section and scattering cross section of particles respectively[21]:

$$\sigma_{\mathrm{abs}} = k\mathrm{Im}[\alpha] = 4\pi k a^3 \mathrm{Im}\left[ \frac{\varepsilon - \varepsilon_m}{\varepsilon + 2\varepsilon_m} \right], \quad (2)$$

$$\sigma_{\mathrm{scat}} = \frac{k^4}{6\pi}|\alpha|^2 = \frac{8}{3}\pi k^4 a^6 \left| \frac{\varepsilon - \varepsilon_m}{\varepsilon + 2\varepsilon_m} \right|^2, \quad (3)$$

where $k$ is the wave vector of incident light. According to Eq. (2) and Eq. (3), $\sigma_{\mathrm{scat}}$ and $\sigma_{\mathrm{abs}}$ will be affected by the dielectric constant $\varepsilon$ of metal material if the dimensionally stable metal particles are in a medium environment with constant $\varepsilon_m$. When the dipole LSPR is excited by $\mathrm{Re}[\varepsilon] = -2\varepsilon_m$, the extinction cross section $\sigma_{\mathrm{ext}}$ of spherical particles is the largest.

According to the Drude-Lorentz dielectric model, the incident light frequency $\omega_{\mathrm{F}}$[21] satisfying the Fröhlich condition is:

$$\omega_{\mathrm{F}} = \sqrt{\frac{\omega_p^2}{1 + \Omega + 2\varepsilon_{\mathrm{m}}} - \tau^2}, \quad (4)$$

where $\omega_p$ is metal plasma frequency; $\Omega$ is the factor of the influence of electronic interband transition on metal dielectric constant[22]; $\omega_p$ and $\Omega$ are both dependent on metal material; $\tau$ is the electron collision frequency, it mainly from electron-electron scattering, phonon-electron scattering and surface-electron scattering, which is influenced by the size of metal structure, the array distribution and the intensity of electron scattering within the material and on the structure surface[21]. As seen from Eq. (4), when $\omega_p$, $\Omega$ and $\tau$ are fixed, $\omega_{\mathrm{F}}$ will decrease as the dielectric constant $\varepsilon_m$ of background environment increases. The corresponding wavelength will register a red shift.

Due to the different complex dielectric constants of various metal materials, the loss responses of incident light in various metals are different. Among them, silver (Ag) and gold (Au) are regarded as ideal materials to enhance the interaction between light and matter based on LSPR effect, due to their small absorption loss[23]. Especially in the visible light bands, compared with the LSP damping frequency of Au ($\Gamma_{\mathrm{Au}}$), Ag has a lower damping frequency $\Gamma_{\mathrm{Ag}}$ and can produce a smaller light absorption loss[24] (particularly obvious in the blue and green bands). According to the physical properties of the above materials, this paper designed an array of Ag nanoparticles (Ag-NPs) to improve the blue light absorption of Si, and calculated the influence of Ag-NP array on the light absorption of Si by using the FDTD algorithm based on Maxwell equations.

### 2.2 Numerical calculation

To simulate the modulation effect of LSPs on the light absorption of silicon, a simplified model of the interaction between metal nanostructure and incident light has been established, as shown in Fig.2 (color online). An Ag-NP array (in silvery white) is arranged on the surface of Si (in red) to form an Ag-NP/Si composite structure.

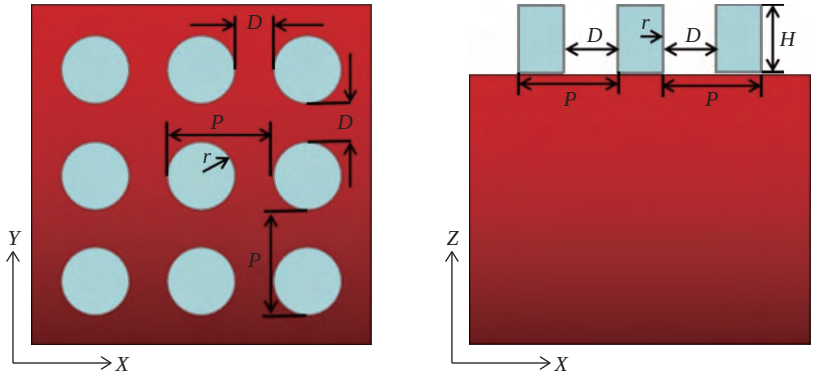


(a) 模型 *XY* 视图
(a) *XY* view of the simulation model

(b) 模型 *XZ* 视图
(b) *XZ* view of the simulation model

Fig. 2 Model structure of Ag-NPs/Si

图 2 Ag-NPs/Si 模型结构

The calculation settings are as follows:

(1) Establish the geometric structure: Si is set as a 20.0 μm-thick cubic structure with smooth surface, while each Ag-NP is set as a cylindrical structure. The dielectric constant of Si is from the data in [25], while that of Ag-NPs is from the data in ref. [26] and is corrected and approximated according to Drude-Lortenz model;

(2) Set the simulation and calculation area: the simulation time is 5 000 fs. Since Ag-NP is a periodic structure on the *XY* plane, the boundary condition is set as follows: the *Z*-axis is the absorption boundary of Perfectly Matched Layer (PML), and the *X*-axis and *Y*-axis are set as anti-symmetry and symmetry respectively.

(3) Select the light source ($\lambda_{in}$): the plane wave with a wavelength range of 380~760 nm and a polarization direction parallel to the *XY* plane is set 1.0 μm away from the upper surface of Si and is incident directly down along the *Z*-axis;

(4) Set the Mesh precision: it is applied to calculate the electromagnetic field distribution of a complex curved surface model structure. A 3D structure is adopted, namely d*x*=d*y*=d*z*=0.3 nm. The geometric area is equal to the size of a single Ag nanoparticle.

The physical model of light absorption of Ag-NPs/Si is simply expressed by the following formula derived from the law of conservation of energy:

$$A_{metal} + A_{Si} + R + T = 1, \qquad (5)$$

where $A_{Si}$ is the light absorptivity of Si; $R$ is the surface reflectivity; $T$ is the transmittance of Si substrate (according to the dispersion properties of silicon[25], the transmission depth for $\lambda$ = 760 nm is about 8.52 μm, while the designed thickness of Si is 20 μm; the incident light can be almost completely absorbed by Si, so the transmittance is considered as $T$ = 0); $A_{metal}$ represents the light absorption loss of Ag-NP array[27]. In this case, the reflectivity $R$ in the incident band and the light absorption loss $A_{metal}$ of metal particles can be accurately calculated by using the FDTD algorithm combined with the material characteristics of Si and Ag[25-26]. Then they are substituted into the Eq. (5) to obtain the light absorptivity of Si, namely $A_{Si} = 1 - R - A_{metal}$, and its gain.

## 3 Results and discussion

### 3.1 Influence of the geometrical parameters of Ag-NPs on the light absorption of Si

Under the action of incident light, metal nanoparticles can scatter and absorb the light, as described by Mie theory[28]. According to Mie theory, the optical response of metal particles to incident

electromagnetic field is shown as follows[28]:

$$E(\lambda)=\frac{24\pi^2 N a^3 \varepsilon_m^{3/2}}{\lambda \ln(10)}\left[\frac{\varepsilon_i}{(\varepsilon_r+\chi\varepsilon_m)^2+\varepsilon_i^2}\right], \quad (6)$$

where $E(\lambda)$ is the extinction spectrum of a metal nanoparticle; $\lambda$ is the incident wavelength; $N$ is the concentration of free electrons in the nanoparticle; $a$ is the particle radius, representing the influence of particle size on extinction properties; $\varepsilon_r$ is the real part of metal dielectric constant; $\varepsilon_i$ is the imaginary part of metal dielectric constant; $\chi$ is the shape factor, usually $\chi = 2$ for a spherical particle, $\chi > 2$[28] for an ellipsoidal particle, showing the correlation between particle geometry and extinction ability. According to Eq. (6), the size and shape of Ag-NPs can influence their extinction spectrum in an environment with constant $\varepsilon_m$. Theoretically, by adjusting the particle size, the LSPR effect can be stimulated in the blue band to improve the blue light absorption of silicon. In addition, given the same incident wavelength, the light absorption gain of Si will also be affected by the modulation effect of geometrical factors on the extinction ability of Ag-NPs. If $G_{abs}$ is the light absorption gain of Si, then:

$$G_{abs}=\frac{A_{Ag-NPs/Si}-A_{Si}}{A_{Si}}\times 100\%, \quad (7)$$

where $A_{Ag\text{-}NPs/Si}$ is the optical absorptance of Si in the Ag-NPs array structure, and $A_{Si}$ is the optical absorptance of single medium Si.

To realize the high blue-light absorption of Si, the Ag-NPs array design is optimized by adjusting the radius $r$, height $H$ and period $P$ of Ag-NPs. In the following calculation process, the optical absorptance of Si in the Ag-NPs array with different geometric parameters in the air will be obtained by using the FDTD algorithm. The material properties of Ag and Si[25-26], the boundary conditions and other settings are the same as those in section 2.2.

3.1.1 Influence of the change of Ag-NP cylinder radius $r$

According to the dipole approximation theory, when the size of metal particles is much smaller than that of the LSPs excited by incident wavelength[28], the particle size $L$ and the resonance wavelength $\lambda_{peak}$ are in the numerical empirical relationship $L$~$0.1\lambda_{peak}$. As the resonance wavelength should be located in the blue band, the radius $r$ of Ag-NP cylinder is preliminarily determined to be within 12.5~22.5 nm according to the above size relation. The step size is set as 2.5 nm, and the height is $H$ = 50.0 nm. In order to remain the coupled intensity of incident light contributed by the interaction polarization of dipolar electromagnetic field within the fixed adjacent Ag-NPs. In Fig.2, the minimum distance $D$ between metal particles is unchanged, $D$ = 20.0 nm. The optical absorptance of Si ($A_{Si}$) calculated by the FDTD method and its variation are shown in Fig.3 (color online).

The Fig.3 (a) shows the optical absorptance of Si in the Ag-NP cylinder array with different radii ($r$). For $r$ = 12.5 nm, 15.0 nm, 17.5 nm, 20.0 nm or 22.5 nm, the maximum optical absorptance of Si is $A_{Si} \approx 74\%$ ($\lambda$ = 451 nm), $A_{Si} \approx 76\%$ ($\lambda$ = 460 nm), $A_{Si} \approx 77\%$ ($\lambda$ = 470 nm), $A_{Si} \approx 78\%$ ($\lambda$ = 479 nm) or $A_{Si} \approx 79\%$ ($\lambda$ = 486 nm) respectively. As seen from the curve, there are two absorption peaks with different intensities in the absorption spectrum of Si. This is similar to the absorption or scattering spectrum of Ag-NPs calculated in refs. [29-35]. According to the $A_{Si}$ defined in Eq. (5), when Ag has a low blue-light absorption loss and the transmittance is ignored, the occurrence of double absorption peaks is mainly related to the change of Ag-NPs extinction ability caused by the shape and structure of metal particles and the dielectric constant of array substrate. As known from the parametric shape factor $\chi$ in Eq. (6), the extinction spectrum of a metal particle depends on its own structure. If the surface structure of a particle is complex with several different symmetry axes, the free electrons in the LSPR state will oscillate inside the particle in different ways. The extinction spectrum reflects multiple

resonance peaks. For example, an ellipsoidal metal nanoparticle has three resonance frequencies because it has three different axes of symmetry[29]. Secondly, according to the Ag-NP extinction spectrum calculated in ref. [35], the single formant in the extinction spectrum will gradually split into two with the increase of the substrate refractivity $n$ if $n > 2$. The analysis result shows that, compared with the common oxide substrates with low refractive index (such as $SiO_2$, $n < 2$), silicon (Si), the substrate material used in this paper, has a higher refractive index and a higher dielectric constant. During the excitation of LSPs, the charges accumulated on the surface of Ag- NPs generate an electric field nearby, causing obvious polarization on Ag-NPs/Si interface that induces the electric field to react upon the metal nanoparticles. This may affect the internal resonance mode and generate double absorption peaks, because LSP is the quantum state of collective electron motion inside the matter in terms of quantum mechanics[9]. Under the polarized electric field at the interface, the wave functions of the quantum states of LSPs inside particles may overlap and cause the quantum interaction, which will affect the extinction performance of Ag-NPs and lead to the phenomenon of double absorption peaks. It is concluded from the above analysis that the geometrical structure of Ag-NPs and the high dielectric constant of the substrate are the main reasons for the occurrence of double peaks on the absorption spectrum of Si.

The Fig.3(b) shows the relationship between the resonance wavelength $\lambda_{peak}$ and the radius $r$. The curve shows that $\lambda_{peak}$ is redshifted with the increase of $r$, which means that $\lambda_{peak}$ increases from 451 nm ($r$ = 12.5 nm) to 486 nm ($r$ = 22.5 nm). The analysis shows that the increase of radius $r$ will cause a longer interaction distance of dipoles in Ag-NPs, a smaller recovery coefficient and a lower resonance frequency of oscillating electrons, and the redshift of LSP formant position[36].

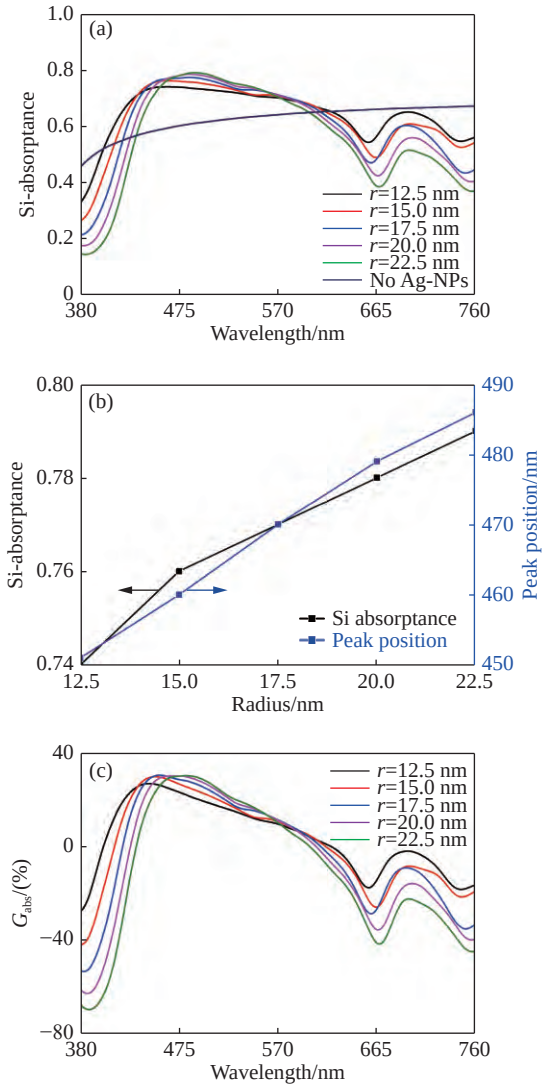


Fig. 3 Influence of geometric parameters of Ag-NPs on the optical properties of silicon. (a) Absorptance versus radius $r$ in blue band; (b) absorptance and resonant wavelength versus radius $r$; (c) absorption gain versus radius $r$ in blue band

图 3 Ag-NPs 几何参数对硅的光学行为的影响。(a)半径 $r$ 对硅在蓝光波段的吸收影响;(b)光吸收率与共振波长随半径 $r$ 的变化;(c)半径 $r$ 对硅在蓝光波段的吸收增益影响

The Fig.3(c) is obtained after substituting the calculation results of Fig.3(a) into Eq. (7). The absorption spectrum lines in the figure indicate that the change of radius $r$ affects the light absorption gain $G_{abs}$ of Si at the same incident wavelength. The analysis of this change shows that, according to Gans theory[37], the extinction coefficient $\sigma_{ext}(\lambda)$ of ellips-

oidal metal nanoparticles can be expressed as:

$$\sigma_{\text{ext}}(\lambda)=\frac{2\pi V\varepsilon_{\text{med}}^{3/2}}{3\lambda}\sum_{j}\frac{\left(1/P_j^2\right)\varepsilon''}{\left(\varepsilon'+\dfrac{1-P_j}{P_j}\varepsilon_{\text{med}}\right)^2+(\varepsilon')^2},\tag{8}$$

where $V$ is the particle volume; $\varepsilon_{\text{med}}$ is the dielectric constant of space environment; $\varepsilon'$ is the real part of dielectric constant of metal particle; $\varepsilon''$ is the imaginary part of dielectric constant of metal particle; $P_j$ represents the polarization factor and is related to the aspect ratio of the particle. According to the extinction coefficient $\sigma_{\text{ext}}(\lambda)$ defined by Eq. (8), not only the volume $V$ but also the aspect ratio (or polarization factor $P_j$) of a particle will change during the adjustment of the radius $r$ (the height $H$ is unchanged). As a result, under the joint modulation of the parameters $V$ and $P_j$, the light absorption gain $G_{\text{abs}}$ of Si in the Ag-NPs with different radii is different.

According to the above analysis, Si has a higher absorption rate ($A_{\text{Si}}$ ≈ 79%) in the blue band ($\lambda$=486 nm) when the radius of Ag-NPs is 22.5 nm ($H$ = 50.0 nm, $P$ = 65.0 nm).

3.1.2　Influence of the change of Ag-NP cylinder height

To further optimize the light absorption gain of Ag-NP array on Si and analyze the change of blue light absorption of Si with the height $H$ of Ag-NP cylinder, we set the radius and period as 22.5 nm and 65.0 nm respectively according to the data results in section 3.1.1. In the range of 30.0 ~ 70.0 nm, the height $H$ was adjusted with the step size of 10.0 nm. The absorption spectra of Si based on the Ag-NP arrays of different heights were calculated with the FDTD algorithm, as shown in Fig.4 (color online).

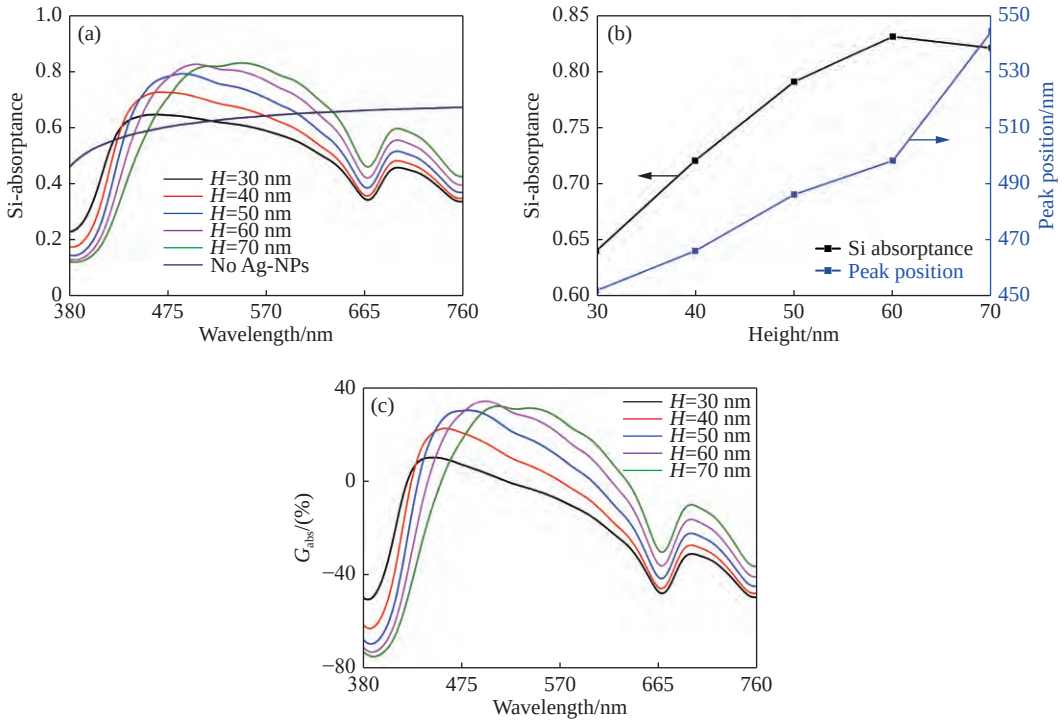


Fig. 4　Influence of geometric parameters of Ag-NPs on the optical properties of silicon. (a) Absorptance versus height $H$ in blue band; (b) absorptance and resonant wavelength versus height $H$; (c) absorption gain versus height $H$ in blue band

图 4　Ag-NPs 几何参数对硅的光学性质的影响。(a)高度 $H$ 对硅在蓝光波段的吸收影响;(b)光吸收率与共振波长随高度 H 的变化;(c)高度 $H$ 对硅在蓝光波段的吸收增益影响

The Fig.4(a) shows the change of Si-absorptance $A_{\text{Si}}$ with the particle height $H$. For $H$ =

30.0 nm, 40.0 nm, 50.0 nm, 60.0 nm or 70.0 nm, the maximum optical absorptance of Si is $A_{Si} \approx 64\%$ ($\lambda$ = 452 nm), $A_{Si} \approx 72\%$ ($\lambda$ = 466 nm), $A_{Si} \approx 79\%$ ($\lambda$ = 486 nm), $A_{Si} \approx 83\%$ ($\lambda$ = 498 nm) or $A_{Si} \approx 82\%$ ($\lambda$ = 544 nm) respectively. The Fig.4(b) shows the relationship between the resonance wavelength $\lambda_{peak}$ and the height $H$. The curve shows that with the increase of Ag-NP height $H$, $\lambda_{peak}$ is redshifted from 452 nm ($H$ = 30.0 nm) to 544 nm ($H$ = 70.0 nm). Because a cylindrical metal nanoparticle has a vertical axis and a horizontal axis, its surface plasma will resonate in two modes in different directions. That is, the vertical surface plasma will resonate in the $y$-direction, while the horizontal surface plasma will resonate in the $x$-direction. The resonance wavelength of surface plasma will shift with the change of aspect ratio[34]. Therefore, the increase of height $H$ will lead to the decrease of electron oscillation frequency and the redshift of formant position.

The light absorption gain in Fig.4(c) is obtained after substituting the calculation results of Fig.4(a) into Eq. (7). The curve in Fig.4(c) shows the influence of height ($H$) change on the light absorption gain $G_{abs}$ at the same incident wavelength. If $H$ = 50.0 nm, the maximum $G_{abs}$ will be 30% at $\lambda$ = 475 nm. If $H$ < 50.0 nm, $G_{abs}$ will increase with the height $H$. If $H$ > 50.0 nm, $G_{abs}$ will decrease with the increasing height $H$. In other words, with the increase of Ag-NP height $H$, $G_{abs}$ will increase first and then decrease. The analysis of this phenomenon based on the Gan theory[37] shows that, the height $H$ (fixed radius $r$) determines the metal nanoparticle volume $V$ and the polarization factor $P_j$, as seen from the extinction coefficient $\sigma_{ext}(\lambda)$ defined by Eq. (8). Both factors jointly modulate the intensity of coupling between incident light and Ag-NPs and affect the extinction ability of Ag-NPs, so that the Ag-NPs with different heights produce different light absorption gains for Si.

According to the above analysis, Si has a higher absorption rate ($A_{Si} \approx 83\%$) in the blue band ($\lambda$=498 nm) when the height of Ag-NPs is 60.0 nm ($r$ = 22.5 nm, $P$ = 65.0 nm).

3.1.3 Influence of the change of Ag-NP array period

In fact, the optical response of a metal nanoparticle array to incident wave depends not only on the material, size, shape and ambient medium of the mono-metal nanoparticles, but also on the distribution of the array particles[38]. To further optimize the light absorption gain effect of Ag-NPs array on Si, the influence of Ag-NPs period $P$ on the blue light absorption of Si was investigated. The period $P$ contains the Ag-NPs diameter 2$r$ and the minimum spacing $D$ between adjacent particles. If the size of Ag-NPs is fixed and $D$ is changed in the optimization process, the coupling intensity of incident light contributed by the interaction between the dipolar fields of adjacent Ag-NPs can be changed to affect the light absorption of Si. According to the calculation results in sections 3.1.1 and 3.1.2, the radius and height were set as $r$ = 22.5 nm and $H$ = 60.0 nm respectively. In the range of 60.0~80.0 nm, the period $P$ was adjusted by a step size of 5.0 nm. The optical absorption spectrum of Si was calculated with the FDTD algorithm. For the results, see Fig.5 (color online).

The Fig.5(a) shows the effect of metal particle period $P$ on the optical absorption spectrum of Si. For $P$ = 60.0 nm, 65.0 nm, 70.0 nm, 75.0 nm or 80.0 nm, the maximum optical absorptance of Si is $A_{Si} \approx 82\%$ ($\lambda$ = 539 nm), $A_{Si} \approx 83\%$ ($\lambda$ = 498 nm), $A_{Si} \approx 80\%$ ($\lambda$ = 486 nm), $A_{Si} \approx 78\%$ ($\lambda$ = 477 nm) or $A_{Si} \approx 75.5\%$ ($\lambda$ = 462 nm). The Fig.5(b) shows the relationship between the resonance wavelength $\lambda_{peak}$ and the period $P$. The curve shows that $\lambda_{peak}$ is blue-shifted from 539 nm ($P$ = 60.0 nm) to 462 nm ($P$ = 80.0 nm). According to the CD-Method theory[39], the dipole polarizability in Ag-NPs has the following relationship with the period:

$$\Pi = \frac{-\boldsymbol{A}E_0}{\omega - \{\omega_o - \mathrm{Re}(\boldsymbol{AS})\} + i\{\gamma + \mathrm{Im}(\boldsymbol{AS})\}}, \quad (9)$$

where $\Pi$ is the dipolar polarizability of metal nano array; $\boldsymbol{A}$ is the dipole action matrix related to the array period, whose modulus is a normal number; $E_0$ is the intensity of external field; $\omega$ is the frequency of incident field; $\omega_0$ is the LSPR frequency of mono-metal nanoparticle, which is influenced by the material, size and geometry of the particle and the dielectric constant of ambient environment[9]; $\gamma$ is the half width of its extinction spectrum; $S$ is the hysteresis dipole [40]. The $AS$ in Eq. (9) changes with the period $P$. According to the CD-Method theory[39], if the period is $P$ < 100 nm, $\omega_0$ and $\gamma$ will remain unchanged and $\lambda_{peak}$ will be blue-shifted with the increase of $P$.

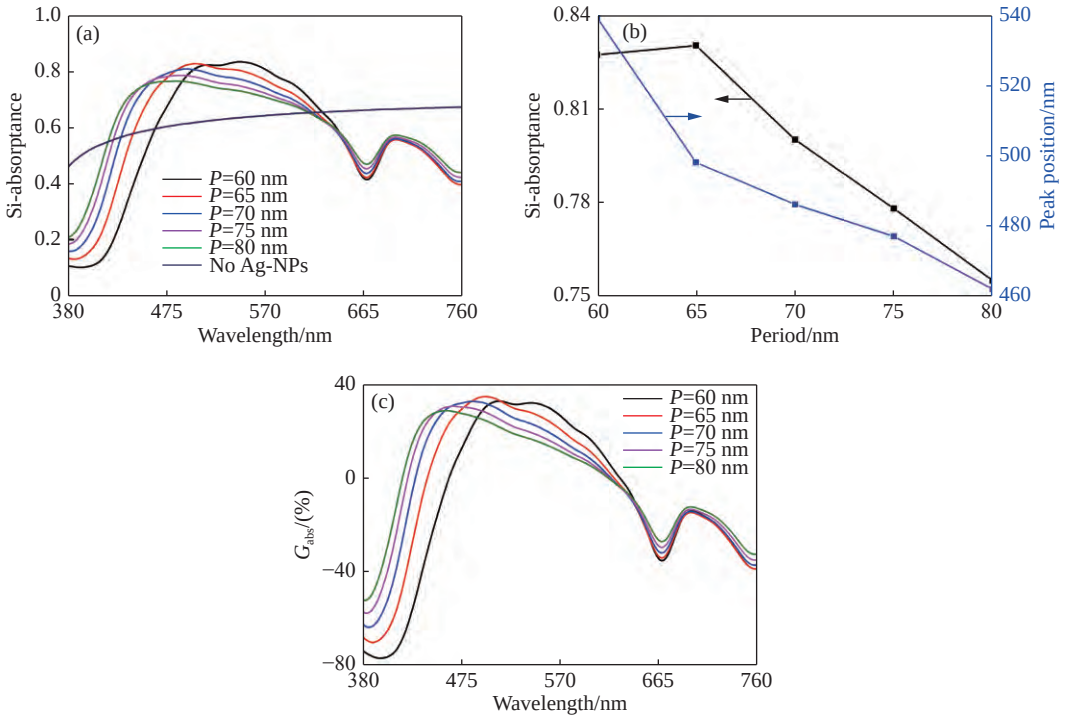


Fig. 5　Influence of geometric parameters of Ag-NPs on the optical properties of silicon. (a) absorptance versus period $P$ in blue band; (b) absorptance and resonant wavelength versus period $P$; (c) absorption gain versus period $P$ in blue band

图 5　Ag-NPs 几何参数对硅的光学性质影响。(a)周期 $P$ 对硅在蓝光波段的吸收影响;(b)光吸收率与共振波长随周期 $P$ 的变化;(c)周期 $P$ 对硅在蓝光波段的吸收增益影响

The light absorption gain of Si in Fig.5(c), namely $G_{abs}$, is obtained after substituting the calculation results of Fig.5(a) into Eq. (7). The curve in Fig.5(c) shows the influence of period ($P$) change on the light absorption gain $G_{abs}$ at the same incident wavelength. If $P$ = 65.0 nm, then $G_{abs}$ will be 34% at the incident wavelength $\lambda$ = 498 nm. If $P$ < 65.0 nm, $G_{abs}$ will increase with $P$. If $P$ > 65.0 nm, $G_{abs}$ will decrease with the increasing $P$. $G_{abs}$ shows a general trend of increasing first and then decreasing. The analysis results show that, the increase of the period $P$ will affect the polarization effect of adjacent particle dipoles[38] and change the intensity of local electromagnetic field in the particle gap. If $P$ = 65.0 nm, the interaction of local electromagnetic fields will maximize the polarizability $\alpha$ of metal particles and the light absorption gain $G_{abs}$ of Si. If $P$ < 65.0 nm, the coupling between dipoles in adjacent Ag-NPs is so strong, that the light absorption loss $A_{metal}$ of Ag-NPs increases and the light absorption of Si and the light absorption gain $G_{abs}$ decreases. If $P$ > 65.0 nm, the interaction between dipoles in adjacent Ag-NPs will decline with the increase of the period $P$. Although the non-radiation

loss effect of Ag-NPs is inhibited[38], the effect of coupling between incident field and Ag-NPs is weakened. The LSP intensity decreases with the increase of the period $P$[38]. As a result, the reflectance $R$ increases and the light absorption gain $G_{abs}$ of Si decreases with the increase of the array period $P$.

According to the above calculation, when the radius, height and period of Ag-NP array are 22.5 nm, 60.0 nm and 65.0 nm respectively, the maximum light absorption rate $A_{Si}$ of Si will be 83% and the absorption peak position will be 498 nm with the peak wavelength at the edge of the blue band. In order to meet the current requirements for efficient blue LED detection, it is necessary to continue to adjust and optimize the design scheme so that the maximum blue light absorption of Si can happen in the range of 440~480 nm.

### 3.2 Light absorption enhancement mechanism of LSPR effect

Based on the above calculation of the influence of Ag-NP geometry parameters on Si absorptance, we repeatedly optimized and calculated the radius $r$, height $H$ and period $P$ of Ag-NPs and the distance $D$ between adjacent particles and finally obtained the following results. If $r$ =18.5 nm, $H$ = 45.0 nm and $P$ = 49.0 nm, the highest light absorption rate of Si in the Ag-NPs/Si composite structure will be approximately 94% and the resonant wavelength will be $\lambda_{peak}$ = 465 nm. The light absorption spectrum of the single medium Si in Fig.6(a) is derived from the calculation results of FDTD algorithm for the interaction between incident light field and Si[25]. From the illustrated calculation results, it is found that in the Ag-NPs/Si structure, Si fails to achieve perfect blue light absorption. The numerical function of Si-absorptance $A_{Si}$ based on Eq. (5) is expressed as: $A_{Si} = 1 - A_{metal} - R$. Due to the light absorption loss $A_{metal}$ and reflectivity $R$ of Ag-NPs, the incident light at the wavelength $\lambda$ = 465 nm is not fully absorbed by Si ($A_{Si}$ < 100%), and double absorption peaks also appear in the absorption spectrum of Si (according to the dispersion characteristics of Si, the design thickness of Si in the Ag-NPs/Si model is much larger than the penetration depth of blue light, so blue light is almost completely absorbed by Si and the transmittance $T$ can be ignored). This phenomenon has been explained previously and will not be explained again. After substituting the calculation results of Fig.6(a) into Eq. (7), the light absorption gain of Si in Fig.6(b) is obtained. At $\lambda$ = 465 nm, the maximum absorption gain is obtained, that is, $G_{abs}$ = 57%.

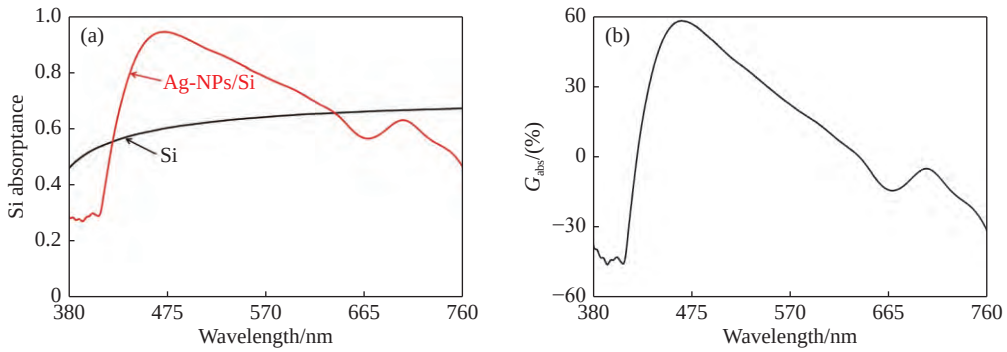


Fig. 6 Si-absorptance in visible bands from 380 nm to 760 nm. (a) Absorptances of silicon without and with Ag-NPs on the surface; (b) absorption gain of silicon

图 6 可见光波段硅的光吸收。(a)硅与基于 Ag-NPs 阵列硅的吸收率曲线;(b)硅的光吸收增益

We explored the influence of LSPR effect on the light absorption of Si in blue band. The analysis results show that, the absorption loss $A_{metal}$ of Ag material in the blue-green band is extremely low[26], and the transmittance can be considered as $T$ = 0 according to the dispersion relation of Si. Therefore, it

can be concluded from Eq. (5) that the enhanced blue light absorption of Si results from the decrease of the surface reflectance $R$ of Si in this band. After the incident light frequency $\omega_{in}$ matches the LSPR frequency $\omega_{LSPR}$ and the equation $\mathrm{Re}[\varepsilon] = -2\varepsilon_m$ is met, the generated LSPR effect provides Ag-NPs with a maximal extinction cross section (or absorption cross section mainly for small particles)[22]. The energy of incident field is converted into the oscillating kinetic energy of dipoles inside the particle to effectively reduce the reflectance $R$ of Si surface. However, according to the polarizability $\alpha$ of metal particles defined in Eq. (1) and the dispersion relation of complex dielectric constant of Ag material[28], the condition $\omega_{in} \neq \omega_{LSPR}$ in the incident band of other frequencies will cause $\mathrm{Re}[\varepsilon] \neq -2\varepsilon_m$, leading to a small polarizability $\alpha$, a lower effect of coupling between incident light and Ag-NPs, a non-resonant state of Ag-NPs and another increase of reflectance $R$ in theory. We detected the reflected light energy 1 μm above the Si surface, and calculated the reflectivity $R$ with the FDTD algorithm under the same calculation conditions, as shown in Fig.7. It can be seen from Fig.6 and Fig.7, when the light at $\lambda_{in} = 465$ nm is incident on the Si surface, its reflectance will be $R_1 \approx 0.41$. According to the Eq. (5), the optical absorptance of Si is $A_1 \approx 0.59$ ($A_{metal} = 0$ if no Ag-NPs exist). When the light is incident on the Ag-NPs/Si structure, the reflectance will drop to $R_2 \approx 0.01$. According to the FDTD numerical method, the light absorption loss of Ag-NPs is calculated to be $A_{metal} \approx 0.05$, as shown in Fig.8. The curve shows that, the theoretical blue-light absorption loss of Ag-NPs is similar to the light absorption loss of 40 nm Ag-NPs calculated by M.A García[34] (see the Fig.8 in ref. [34]). After substituting the light absorption loss $A_{metal}$ of Ag-NPs into Eq. (5), the optical absorptance of Si in the Ag-NPs array is determined as $A_2 \approx 0.94$, higher than $A_1$ ($A_1 \approx 0.59$). From the curve in Fig.8, we also find that although the light absorption loss $A_{metal}$ at $\lambda > 465$ nm is smaller than 0.05, the reflectance $R$ is still increasing, as shown in the reflectance curve of Fig.7. As a result, the optical absorptance of Si calculated by Eq. (5) is $A_{Si} < 0.94$. For example, if $\lambda = 475$ nm, $R = 0.04$ and $A_{metal} = 0.03$, the optical absorptance calculated by the above Equation (5) will be $A_{Si} \approx 0.93$.

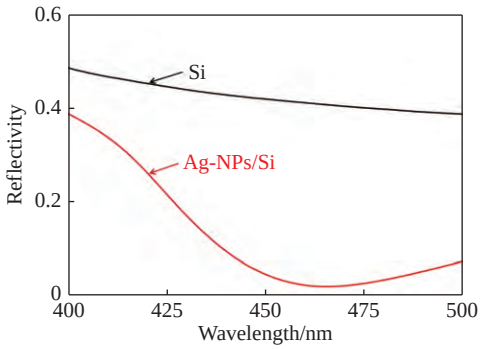


Fig. 7　Reflectivity $R$ of structure surface in blue band versus absorption loss $A_{metal}$ of Ag-NPs

图 7　蓝光波段结构表面反射率 $R$ 与 Ag-NPs 光吸收损耗 $A_{metal}$ 的关系曲线

It can be seen from the above data that the LSPR effect reduces the reflectivity of Si surface, and that most of the incident light energy is coupled by Ag-NPs into the interior of Si and then absorbed by Si.

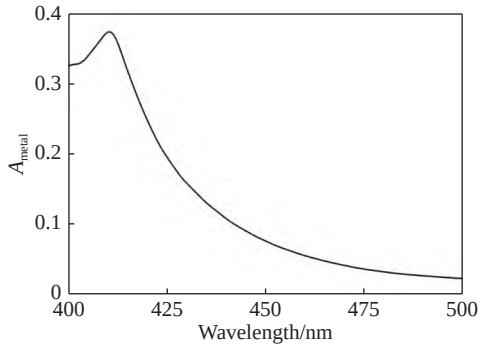


Fig. 8　Absorption loss $A_{metal}$ of Ag-NPs in blue band

图 8　蓝光波段 Ag-NPs 光吸收损耗 $A_{metal}$ 曲线

### 3.3　Gain effect of Ag-NPs array on photo-generated carriers

The number of generated carriers has a certain effect on the quantum efficiency of semiconductor photodetectors. If the production rate of electron-

hole pairs, namely $G_e(x)$, is used to represent the number of photo-generated carriers[41], then:

$$G_e(x) = \Phi_0 \alpha \exp(-\alpha x) = \frac{(1-R)P_{opt}}{S \cdot h\upsilon} \alpha \exp(-\alpha x), \quad (10)$$

where $\Phi_0$ is incident photon flux, $R$ is reflectivity, $P_{opt}$ is incident light power (W/m$^2$), $S$ is incident area (m$^2$), $h\upsilon$ is single-photon energy (eV), and $\alpha$ is the absorption coefficient of a medium (m$^{-1}$). The power density of incident light is 1 W/m$^2$. Depending on the optical absorption energy (internal energy loss of undirected air propagation) of silicon is all converted into hole-electron pairs. The calculation conditions are the same as those in section 2.2. By using the FDTD algorithm and Eq. (10), we calculated the number of initial photo-generated carriers of Si in the Ag-NP array under the conditions $\lambda_{in}$ = 465 nm, $r$ = 18.5 nm, $H$ = 45.0 nm and $P$ = 49.0 nm. The results are shown in Fig.9(a), where the horizontal axis represents the propagation distance of incident light within Si. The comparison of carrier generation rates in Fig. 9(a) shows that the LSPR effect can increase the number of photo-generated carriers in Si, and indirectly indicates that a certain number of photo-generated carriers can be generated in the depths of silicon.

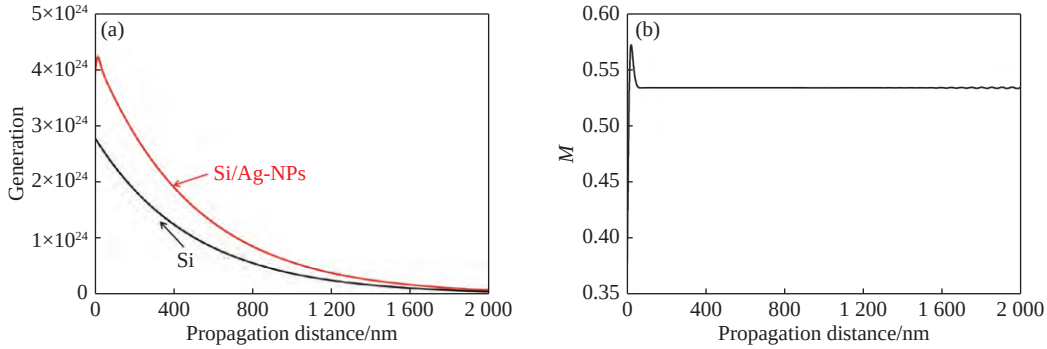


Fig. 9 Generation rate of carriers at $\lambda_{in}$ = 465 nm: (a) carrier generation rates of Si/Ag-NPs and Si; (b) gain ratio

图 9 入射波长 465 nm 载流子数量曲线:(a)载流子数量曲线;(b)载流子增益比

If $G$ is the number of photo-generated carriers (m$^{-3}$) and $M$ is the gain ratio of $G$, then:

$$M = \frac{G_{Ag-NPs/Si} - G_{Si}}{G_{Si}}, \quad (11)$$

where $G_{Ag\text{-}NPs/Si}$ and $G_{Si}$ are the concentrations of photo-generated carriers in Ag-NPs/Si structure and single medium Si respectively. After substituting the number of photo-generated carriers ($G$) calculated in Fig.9(a) into Eq. (11), the gain of $G$ in the Ag-NPs/Si structure is determined as $M \approx 0.53$, as shown in Fig.9(b). According to the analysis of $G_e(x)$ defined in Eq. (10), $M$ is caused by the decrease of the reflectivity $R$ of Ag-NPs/Si structure. The physical mechanism of this change has been explained in the previous section, so it will not be repeated here. Therefore, the following conclusion is drawn: theoretically, the LSPR effect can increase the number of photo-generated carriers and the probability of carrier collection by electrodes, and enhance the quantum efficiency of Si-based photodetectors.

The above research results have important theoretical reference value for the design of silicon-based visible light photodetectors with high blue-light response and for the solution to other issues.

## 4 Conclusion

The effect of Ag-NPs/Si composite structure on visible light absorption was studied in this paper. In the blue band, the relations between the geometrical

parameters (radius $r$, height $H$ and period $P$) of Ag-NPs and the light absorption of Si were calculated separately. When the radius $r$ is increased, the optical absorptance of Si will increase and the formant position will register a redshift. When the height $H$ is increased, the optical absorptance of Si will increase first and then decrease and the formant position will register a redshift. When the period $P$ is increased, the optical absorptance of Si will increase first and then decrease and the formant position will register a blueshift. The optimization results of Ag-NPs/Si composite structure show that when the parameters of Ag-NPs structure are $r$ = 18.5 nm, $H$ = 45.0 nm and period $P$ = 49.0 nm, the maximum absorption rate of Si will be 94%, the maximum absorption peak wavelength will be $\lambda$ = 465 nm, and the light absorption gain will be 0.57. The calculated gain of the number of photo-generated carriers of Ag-NPs/Si at $\lambda$ = 465 nm is approximately 0.53. The enhancement of optical absorptance of Si and the increase of the number of photo-generated carriers are related to the decrease of surface reflectivity of Si caused by LSPR effect. The research results have high reference value for the design of silicon-based visible light photodetectors using Ag-NPs to enhance the blue light response.

——中文对照版——

## 1　引　言

近年来，随着表面等离激元（Surface Plasmons, SPs）理论的不断发展和微纳加工技术的不断提高，基于 SPs 对光电探测器的增敏研究[1] 引起研究人员的极大兴趣。SPs 具有提高局域电磁场强度、增强光与物质相互作用[2]、选择光吸收、超高的吸收率[3] 等特点，使其在太阳能电池[4]、LED[5-6]、表面增强拉曼光谱[7]、光电探测[8] 等领域的应用受到广泛关注。

微纳阵列的材料性质、几何形状、结构参数、介质背景等因素会对 SPs 的物理现象产生影响[9]，材料自身性质决定了 SPs 的主要衰减途径，导致 SPs 对光电探测器的增敏方式不同[10]，例如金纳米颗粒 (Au-Nanoparticles, Au-NPs) 在发生表面等离激元共振 (Surface Plasmons Resonance, SPR) 衰减时通过朗道阻尼将吸收的光能量传递给金属内的自由电子，自由电子转换为热电子并跃过肖特基势垒注入半导体，提高入射波段光响应度；SPR 在银纳米颗粒 (Ag-Nanoparticles, Ag-NPs)、铝纳米颗粒 (Aluminum-Nanoparticles, Al-NPs) 的衰减模式是将入射光能量以光辐射的形式向介质散射[11]，以提高金属颗粒基底的光吸收率，增强光电探测器的光电性能。

2011 年，Naomi Halas 课题组[12] 证实基于 Au-nanorods 实现入射光子能量低于硅带隙宽度 $E_g$ 的热电子探测，光电流增加 20 倍（入射光 $\lambda_{in}$ = 1.4 μm）；2012 年，Li 课题组[13] 研究了表面等离激元效应与 GaN 基探测器耦合的光电响应性能，通过在 GaN 表面制备尺寸不均匀的 Ag 纳米颗粒，使器件响应度提高 30 倍（入射光 $\lambda_{in}$ = 0.36 μm）；2013 年，Sobhani 等人[14] 在 Si 表面制备 Au 光栅，基于光学异常透射 (Extraordinary Optical Transmission, EOT) 效应的硅基热电子探测器的光响应度为 0.6 mA/W（入射光 $\lambda_{in}$ = 1.46 μm），内量子效率为 0.2%；2014 年，Bao 等[15] 研究基于不均匀密度 Al-NPs 的 AlGaN 基日盲紫外探测器光电性能增益，通过激发表面等离激元增强 AlGaN 探测器的性能，使光响应度从 0.144 A/W 增至 0.288 A/W（入射光 $\lambda_{in}$ = 0.288 μm）。上述研究工作表明金属微纳结构激发的 SPs 效应，一方面增加了探测器对入射光子的捕获及产生空穴—电子对与光电流的概率，另一方面基于热电子效应，通过穿越肖特基势垒显著提高了光电流产生的效率，有效增强光电探测器在响应波段内的工作性能。

硅（Si）在 380~1 100 nm 入射波段具有被激发载流子的宽光谱响应能力，然而由于蓝光波段

Si 的吸收系数相对较大、透入深度小，导致光生载流子易扩散至界面或表面态[16]，使扩散和漂移至耗尽区的光生载流子数目少，造成硅基光电探测器（Silicon Photodetector, Si-PD）在该波段量子效率和光响应度较低。而 Si 基高效蓝光探测器在可见光通信[17]、水下通信[18]、局域智能定位[19]等领域拥有极大的潜在应用市场。

目前，有关基于 SPs 增强 Si-PD 蓝光波段光电性能的研究报道的很少。基于此，本文在硅表面设计金属纳米颗粒阵列，基于有限时域差分法(Finite-Difference-Time-Domain, FDTD)[20]，研究不同几何参数的金属纳米粒子对 Si 的光吸收特性的影响，根据局域表面等离激元 (Localized Surface Plasmons, LSPs) 的物理性质[9]对结果进行分析。希望通过研究 SPs 对 Si 在蓝光波段的光吸收影响，提高硅的蓝光吸收，为设计制备基于 SPs 增强的具有高蓝光探测效率的 Si 基光探测器提供参考。

## 2 理论模型

### 2.1 局域表面等离激元与 FDTD 数值算法

若金属颗粒的尺寸远小于入射场的穿透深度，自由电子在库伦场与外电磁场的共同作用下相对金属晶格发生振荡，由此产生的非传播混合激发态为局域表面等离激元[9]，如图 1 所示。

以直径小于 100 nm 的金属纳米球形颗粒为例，在准静态近似下，极化率 $\alpha$ 可用于描述入射光与粒子的相互作用，表征局域表面等离激元强度，表达式为：

$$\alpha = 4\pi a^3\left(\frac{\varepsilon-\varepsilon_m}{\varepsilon+2\varepsilon_m}\right), \tag{1}$$

式中，$a$ 为颗粒半径，$\varepsilon_m$ 为背景环境的相对介电常数，$\varepsilon$ 为金属粒子的相对复介电常数，受入射电磁场频率、材料特性、尺寸等因素影响。公式(1)表明当 $\mathrm{Re}[\varepsilon]=-2\varepsilon_m$ 时，极化率 $\alpha$ 极大，激发局域表面等离激元共振（Localized Surface Plasmons Resonance, LSPR）现象，$\mathrm{Re}[\varepsilon]=-2\varepsilon_m$ 也称为 Fröhlich 条件[9]。金属纳米粒子处于 LSPR 状态时的极化率、吸收及散射入射光效率最大，通常用消光截面 $\sigma_{\mathrm{ext}}$ 表征其光学总响应，则有如下数值关系：$\sigma_{\mathrm{ext}}=\sigma_{\mathrm{abs}}+\sigma_{\mathrm{scat}}$，其中，$\sigma_{\mathrm{abs}}$ 与 $\sigma_{\mathrm{scat}}$ 分别为颗粒的光学吸收截面和散射截面[21]，

$$\sigma_{\mathrm{abs}} = k\mathrm{Im}[\alpha] = 4\pi k a^3 \mathrm{Im}\left[\frac{\varepsilon-\varepsilon_m}{\varepsilon+2\varepsilon_m}\right], \tag{2}$$

$$\sigma_{\mathrm{scat}} = \frac{k^4}{6\pi}|\alpha|^2 = \frac{8}{3}\pi k^4 a^6\left|\frac{\varepsilon-\varepsilon_m}{\varepsilon+2\varepsilon_m}\right|^2, \tag{3}$$

式中，$k$ 为入射光波矢。根据式(2)与式(3)可知，若尺寸不变的金属粒子在 $\varepsilon_m$ 恒定的介质环境中，$\sigma_{\mathrm{scat}}$ 与 $\sigma_{\mathrm{abs}}$ 受金属材料介电常数 $\varepsilon$ 的影响，这种情况，当 $\mathrm{Re}[\varepsilon]=-2\varepsilon_m$，激发偶极 LSPR 现象时，球形颗粒的消光截面 $\sigma_{\mathrm{ext}}$ 最大。

根据 Drude-Lorentz 介电模型，满足 Fröhlich 条件的入射光频率 $\omega_{\mathrm{F}}$[21] 为：

$$\omega_{\mathrm{F}} = \sqrt{\frac{\omega_p^2}{1+\Omega+2\varepsilon_m}-\tau^2}, \tag{4}$$

式中，$\omega_p$ 为金属等离子体频率，$\Omega$ 为电子带间跃迁对金属介电常数的影响因子[22]，$\omega_p$ 和 $\Omega$ 均与金属材料相关，$\tau$ 为电子碰撞频率，其碰撞主要源于电子—电子散射、声子—电子散射和表面—电子散射，频率大小受金属结构尺寸、阵列分布和材料内部及结构表面对电子散射强度的影响[21]。通过公式(4)可看出，$\omega_p$、$\Omega$ 与 $\tau$ 固定，$\omega_{\mathrm{F}}$ 随背景环境介电常数 $\varepsilon_m$ 的增加而降低，对应的波长红移。

由于各金属材料的复介电常数等特性不同，入射光在金属内的损耗响应具有差异性，其中银材料（Ag）、金材料（Au）因较小的吸收损耗被视为基于 LSPR 效应增强光与物质相互作用的理想材料[23]，特别是在可见光波段，与 Au 材料的 LSPs 阻尼频率 $\Gamma_{\mathrm{Au}}$ 相比，Ag 材料具有低阻尼频率 $\Gamma_{\mathrm{Ag}}$，可产生更小的光吸收损耗[24]（蓝绿波段尤为明显）。根据上述材料的物理性质，本文通过设计银纳米颗粒 (Ag-NPs) 阵列结构，提高 Si 的蓝光吸收，并基于 Maxwell 方程组的 FDTD 数值算法计算 Ag-NPs 阵列对 Si 光吸收的影响。

### 2.2 数值计算

为模拟 LSPs 对硅光吸收的调制作用，建立了金属纳米结构与入射光相互作用的简化模型，如图 2（彩图见期刊电子版）。在 Si（红色部分）表

面设置 Ag-NPs 阵列(银白色部分), 形成 Ag-NPs/Si 复合结构。

计算设置如下:

(1)建立几何结构: Si 设置为表面光滑的立方体结构, Ag-NPs 设置为圆柱体结构, Si 厚度为 20.0 μm, Si 的介电常数源自文献 [25] 数据, Ag-NPs 的介电常数源于文献 [26] 数据, 并根据 Drude-Lortenz 模型进行修正近似;

(2)设置仿真计算区域: 仿真时间为 5 000 fs。由于 Ag-NPs 在 *XY* 面是周期性结构, 边界条件设置为: *z* 轴方向为完美匹配层(Perfectly matched layer, PML)吸收边界, *x* 轴和 *y* 轴分别设置为反对称(Anti-symmetry)和对称(Symmetry);

(3)选取光源 ($\lambda_{in}$) 是波长范围为 380~760 nm、偏振方向平行于 *XY* 面的平面波 (Plane Wave), 设置于距 Si 上表面 1.0 μm 处、沿 *z* 轴向下正入射;

(4)Mesh 精度设置: 应用于计算复杂曲面模型结构的电磁场分布, 采用 3D 结构, d*x*=d*y*=d*z*=0.3 nm, 几何区域设置等于单 Ag 纳米颗粒尺寸。

Ag-NPs/Si 的光吸收物理模型用能量守恒定律的衍生公式简化表达:

$$A_{\text{metal}} + A_{\text{Si}} + R + T = 1, \tag{5}$$

式中, $A_{\text{Si}}$ 为 Si 的光吸收率, $R$ 为表面反射率, $T$ 为 Si 衬底的透射率(根据硅的色散特性[25], $\lambda$ = 760 nm 时的透射深度约为 8.52 μm, 而 Si 的设计厚度为 20 μm, 入射光可被 Si 几乎全部吸收, 认为透射率 $T = 0$), $A_{\text{metal}}$ 表示 Ag-NPs 阵列的光吸收损耗[27]。在这种情况下, 根据 FDTD 算法, 结合 Si 及 Ag 的材料特性[25-26], 准确计算入射波段内反射率 $R$ 与金属颗粒的光吸收损耗 $A_{\text{metal}}$, 代入式(5)得出 Si 的光吸收率 $A_{\text{Si}}$ (=1 − $R$ − $A_{\text{metal}}$) 及其增益。

## 3　结果与讨论

### 3.1　Ag-NPs 的几何参数对 Si 光吸收的影响

金属纳米颗粒在入射光的作用下, 存在光的散射与吸收现象, Mie 理论已对其光学响应过程做出描述[28]。根据 Mie 理论, 金属颗粒对入射电磁场的光响应关系式如下[28]:

$$E(\lambda) = \frac{24\pi^2 N a^3 \varepsilon_m^{3/2}}{\lambda \ln(10)} \left[ \frac{\varepsilon_i}{(\varepsilon_r + \chi\varepsilon_m)^2 + \varepsilon_i^2} \right], \tag{6}$$

式中, $E(\lambda)$ 表示金属纳米粒子的消光光谱, $\lambda$ 为入射波长, $N$ 为纳米颗粒的自由电子浓度, $a$ 为颗粒尺寸半径, 表征颗粒尺寸对消光性质的影响, $\varepsilon_r$ 为金属介电常数实部, $\varepsilon_i$ 为金属介电常数虚部, $\chi$ 为形状因子, 用于表征颗粒几何形状与消光能力的关联性。通常, 对于球形颗粒 $\chi = 2$, 对于椭圆球体 $\chi > 2$[28]。公式(6)表明: 在 $\varepsilon_m$ 恒定的环境内, Ag 纳米颗粒的尺寸与形状会影响 Ag-NPs 的消光光谱。理论上通过调节粒子大小可在蓝光波段激发 LSPR 效应, 提高硅的蓝光吸收率, 并且在同一入射波长下, 由于几何因素对 Ag-NPs 消光能力的调制作用, 使 Si 的光吸收增益效果也受到影响, 设 $G_{\text{abs}}$ 为 Si 的光吸收增益:

$$G_{\text{abs}} = \frac{A_{\text{Ag-NPs/Si}} - A_{\text{Si}}}{A_{\text{Si}}} \times 100\%, \tag{7}$$

式中, $A_{\text{Ag-NPs/Si}}$ 为基于 Ag-NPs 阵列结构 Si 的光吸收率, $A_{\text{Si}}$ 为单一介质 Si 的光吸收率。

为实现 Si 的高蓝光吸收, 分别通过调节 Ag 纳米颗粒的半径 $r$、高度 $H$ 与周期 $P$, 优化 Ag 纳米颗粒阵列。在下列计算过程中, 基于 FDTD 算法得到在空气中不同几何参数的 Ag-NPs 阵列对 Si 的光吸收率, 其中 Ag 与 Si 的材料性质[25-26]、边界条件等与 2.2 节相同。

#### 3.1.1　Ag 纳米圆柱半径 *r* 变化的影响

根据偶极子近似理论, 当金属颗粒尺寸远小于入射光波长激发 LSPs 时[28], 可认为粒子大小 $L$ 与共振波长 $\lambda_{\text{peak}}$ 具有 $L \sim 0.1\lambda_{peak}$ 的数值经验关系。由于共振波长需位于蓝光波段, 根据上述尺寸关系, 初步确定 Ag 纳米圆柱半径 $r$ 的变化范围在 12.5 ~ 22.5 nm 内, 并以 2.5 nm 步长调节, 设高度 $H$ = 50.0 nm。使相邻 Ag 纳米颗粒内偶极电磁场的相互极化作用对入射光的耦合强度固定, 图 2 中金属颗粒最小间距 $D$ 不变, 设 $D$ = 20.0 nm。基于 FDTD 数值方法计算得到 Si 的光吸收率 $A_{\text{Si}}$ 及其变化情况, 如图 3(彩图见期刊电子版)所示。

图 3(a)给出了不同半径 $r$ 的 Ag 纳米圆柱阵列 Si 的光吸收率, 可见, 当 $r$ 分别为 12.5、15.0、

17.5、20.0 与 22.5 nm 时, Si 的最高光吸收率分别为 $A_{Si}\approx 74\%$ ($\lambda=451$ nm)、$A_{Si}\approx 76\%$ ($\lambda=460$ nm)、$A_{Si}\approx 77\%$ ($\lambda=470$ nm)、$A_{Si}\approx 78\%$ ($\lambda=479$ nm) 与 $A_{Si}\approx 79\%$ ($\lambda=486$ nm)。通过图中曲线发现, Si 的光吸收谱存在两个强度不同的吸收峰, 文献 [29-35] 计算得到的 Ag-NPs 的吸收或散射光谱也具有类似情况。在 Ag 具有较低的蓝光吸收损耗并忽略透射率的情况下, 分析认为 Si 的双吸收峰现象主要是与由金属粒子的形状结构、阵列衬底的介电常数大小引起的 Ag-NPs 消光特性变化相关。根据参数形状因子 $\chi$ 定义可知, 金属颗粒的消光光谱依赖于自身结构, 若粒子的曲面结构较为复杂、具有多个不同的对称轴时, 处于 LSPR 状态的自由电子在其内部会产生不同的振荡模式, 消光谱反映出多个共振峰, 例如: 椭球型金属纳米颗粒因具有 3 个不同的对称轴会产生 3 个共振频率[29]; 其次, 根据文献 [35] 计算的 Ag-NPs 消光谱发现, 当衬底折射率 $n>2$ 时, 随着 $n$ 的增加, 消光谱的单共振峰逐渐分裂为双共振峰, 分析认为, 与常见低折射率氧化物(例如: $SiO_2$, $n<2$)衬底相比, 本文使用的衬底材料—Si 的折射率较高、介电常数较大, 在激发 LSPs 的过程中, Ag 纳米颗粒表面积累的电荷在附近产生电场, 使 Ag-NPs/Si 的界面出现较明显的极化现象, 诱导电荷形成的电场反作用金属纳米粒子, 可能会影响内部的共振模式而产生双吸收峰现象, 因为从量子力学的角度看, LSPs 是物质内部电子集体运动的量子态[9], 在界面处极化电场作用下, 颗粒内 LSPs 量子态的波函数可能会发生重叠而引起量子相互作用, 使 Ag-NPs 的消光特性受到影响而产生双吸收峰现象。结合上述分析认为, Ag 纳米颗粒的几何结构与衬底较高的介电常数是 Si 的光吸收谱出现双峰现象的主要原因。

图 3(b)展示了共振波长 $\lambda_{peak}$ 与半径 $r$ 的变化关系, 通过图中曲线可看出: $\lambda_{peak}$ 随 $r$ 的增加而发生红移的物理现象, 即 $\lambda_{peak}$ 从 451 nm ($r$ = 12.5 nm) 增加至 486 nm ($r$ = 22.5 nm)。分析认为, 半径 $r$ 的增加使 Ag-NPs 内偶极子的相互作用距离延长, 导致振荡电子回复系数减小、共振频率降低, 引起 LSPs 共振峰位红移[36]。

将图 3(a)的计算结果代入公式(7)可得到图 3(c), 图中的吸收谱线表明半径 $r$ 的变化使同一入射波长下 Si 的光吸收增益 $G_{abs}$ 受到影响。对于该变化关系, 根据 Gans 理论[37], 金属纳米椭球颗粒的消光系数 $\sigma_{ext}(\lambda)$ 可表示为:

$$\sigma_{ext}(\lambda)=\frac{2\pi V\varepsilon_{med}^{3/2}}{3\lambda}\sum_j\frac{\left(1/P_j^2\right)\varepsilon''}{\left(\varepsilon'+\frac{1-P_j}{P_j}\varepsilon_{med}\right)^2+(\varepsilon')^2}, \tag{8}$$

式中, $V$ 表示颗粒体积, $\varepsilon_{med}$ 表示空间环境介电常数, $\varepsilon'$表示金属颗粒介电常数实部, $\varepsilon''$表示金属颗粒介电常数虚部, $P_j$ 表示极化因子, 与颗粒的横纵轴比有关。式(8)定义的消光系数 $\sigma_{ext}(\lambda)$ 表明, 在调节半径 $r$(高度 $H$ 不变)的过程中, 不仅颗粒体积 $V$ 发生变化, 也造成颗粒纵横比即极化因子 $P_j$ 的改变, 导致消光系数 $\sigma_{ext}(\lambda)$ 在参数 $V$ 与 $P_j$ 共同调制作用下, 使不同半径 $r$ 的 Ag 纳米颗粒对 Si 的光吸收增益 $G_{abs}$ 具有差异性。

上述计算数据分析认为, 当 Ag-NPs 半径 $r$ = 22.5 nm(高度 $H$ = 50.0 nm, 周期 $P$ = 65.0 nm)时, Si 在蓝光 $\lambda$=486 nm 波段具有较高的光吸收率 $A_{Si}\approx 79\%$。

### 3.1.2 Ag 纳米圆柱高度变化的影响

为进一步优化 Ag-NPs 阵列对 Si 的光吸收增益效果, 探究 Si 的蓝光吸收随 Ag 纳米圆柱高度 $H$ 的变化情况, 根据 3.1.1 节的数据结果, 半径与周期分别固定为 $r$ = 22.5 nm 与 $P$ = 65.0 nm, 在 30.0~70.0 nm 范围内以 10.0 nm 为步长调节高度 $H$, 根据 FDTD 算法计算得到基于不同高度 Ag 纳米颗粒阵列 Si 的光吸收谱, 如图 4 所示。

图 4(a)展示了 Si 的光吸收率 $A_{Si}$ 随调节颗粒高度 $H$ 的变化情况, 当 $H$ 分别为 30.0、40.0、50.0、60.0 与 70.0 nm 时, Si 的最高光吸收率分别为 $A_{Si}\approx 64\%$ ($\lambda=452$ nm)、$A_{Si}\approx 72\%$ ($\lambda=466$ nm)、$A_{Si}\approx 79\%$ ($\lambda=486$ nm)、$A_{Si}\approx 83\%$ ($\lambda=498$ nm) 与 $A_{Si}\approx 82\%$ ($\lambda=544$ nm)。图 4(b)给出了共振波长 $\lambda_{peak}$ 与高度 $H$ 的变化关系, 图中曲线表明 $\lambda_{peak}$ 随 Ag-NPs 高度 $H$ 的增加而红移, $\lambda_{peak}$ 由 452 nm ($H$ = 30.0 nm) 红移至 544 nm ($H$ = 70.0 nm)。由于金属圆柱状纳米颗粒存在纵轴和横轴, 其结构决定了其有两种不同方向的表面等离激元共振

模式: 沿纵轴方向的纵向表面等离激元与沿横轴方向的横向表面等离激元模式。表面等离激元模式的共振波长会随着横纵宽度比的变化而偏移[34], 因此高度 $H$ 的增加导致电子振荡频率降低, 从而导致共振峰位发生红移。

将图 4(a)的计算结果代入公式(7)得到图 4(c)的光吸收增益, 图中曲线展示了在同一入射波长下, 高度 $H$ 变化对 Si 的光吸收增益 $G_{abs}$ 的影响。可见: 在 $\lambda$ = 475 nm 处, 当 $H$ = 50.0 nm 时, $G_{abs}$ 最高为 30%; 当 $H$ < 50.0 nm时, $G_{abs}$ 随高度 $H$ 的增加而增加; 当 $H$ > 50.0 nm 时, $G_{abs}$ 随高度 $H$ 的增加而降低, 即随着 Ag-NPs 高度 $H$ 的增加, $G_{abs}$ 表现出先增大后减小的趋势。对于此现象, 结合 Gan 理论[37] 进行分析: 由式(8)消光系数 $\sigma_{ext}(\lambda)$ 的定义可知, 金属纳米颗粒体积 $V$ 与极化因子 $P_j$ 共同调制入射光与 Ag-NPs 的耦合强度, 影响 Ag-NPs 的消光能力, 而高度 $H$(固定半径 $r$)决定了金属纳米颗粒体积 $V$ 与极化因子 $P_j$ 的大小, 从而使不同高度 $H$ 的 Ag 纳米颗粒对 Si 的光吸收增益具有差异性。

根据上述分析可知, 当 Ag-NPs 高度 $H$ = 60.0 nm (半径 $r$ = 22.5 nm, 周期 $P$ = 65.0 nm)时, Si 在蓝光 $\lambda$=498 nm 处具有较高的光吸收率, 为 $A_{Si} \approx$ 83%。

### 3.1.3　Ag 纳米圆柱阵列周期变化的影响

实际上, 金属纳米颗粒阵列对入射波光响应的影响不仅取决于单金属纳米颗粒的材质、尺寸、形状与周围的环境介质, 阵列颗粒的分布状况也会影响入射光场的变化[38]。为更进一步优化 Ag-NPs 阵列对 Si 的光吸收增益效果, 探究 Ag 纳米颗粒周期 $P$ 对 Si 蓝光吸收的影响。由于 $P$ 包含 Ag 纳米颗粒直径 2$r$ 和相邻粒子最小间距 $D$ 的信息, 若使 Ag-NPs 尺寸固定, 在优化过程中使 $D$ 发生变化, 改变相邻 Ag 纳米颗粒偶极场之间的相互作用对入射光的耦合强度, 从而影响 Si 的光吸收。根据 3.1.1 与 3.1.2 节的计算结果, 半径与高度分别固定为 22.5 nm 和 60.0 nm, 在 60.0 ~80.0 nm内以 5.0 nm 步长调节周期 $P$ 值, 根据 FDTD 算法计算 Si 的光吸收谱, 结果如图 5 (彩图见期刊电子版)所示。

图 5(a)展示了金属颗粒周期 $P$ 对 Si 的光吸收谱的影响, 当 $P$ 分别为 60.0、65.0、70.0、75.0 与 80.0 nm 时, Si 的最高光吸收率分别为 $A_{Si} \approx$ 82% ($\lambda$ = 539 nm)、$A_{Si} \approx$ 83% ($\lambda$ = 498 nm)、$A_{Si} \approx$ 80% ($\lambda$ = 486 nm)、$A_{Si} \approx$ 78% ($\lambda$ = 477 nm)与 $A_{Si} \approx$ 75.5% ($\lambda$ = 462 nm)。图 5(b)给出了共振波长 $\lambda_{peak}$ 与周期 $P$ 的关系, 由图中曲线可以看出, $\lambda_{peak}$ 由 539 nm ($P$ = 60.0 nm) 蓝移至 462 nm ($P$ = 80.0 nm)。根据 CD-Method 理论[39], Ag 纳米颗粒内偶极子极化率与周期具有如下的关系:

$$\Pi = \frac{-\boldsymbol{A}E_0}{\omega - \{\omega_o - \mathrm{Re}(AS)\} + i\{\gamma + \mathrm{Im}(AS)\}}, \qquad (9)$$

式中, $\Pi$表示金属纳米阵列的偶极子极化率, $\boldsymbol{A}$ 是与阵列周期相关的偶极子作用矩阵, 模为正常数, $E_0$ 是外场强度, $\omega$ 表示入射场频率, $\omega_0$ 表示单金属纳米颗粒的局域表面等离激元共振频率, 其受颗粒的材料、尺寸与几何形状及其所处周围环境的介电常数有关[9]。$\gamma$ 为其消光光谱半宽度, $S$ 表示迟滞偶极子[40]。周期 $P$ 的变化使式(9)中的 $AS$ 发生改变, 根据 CD-Method 理论[39], 在周期 $P$ < 100 nm 时, $\omega_0$ 与 $\gamma$ 固定不变, $\lambda_{peak}$ 会随周期 $P$ 的增加而发生蓝移。

将图 5(a)的计算结果代入式(7)可得到图 5(c)所示的 Si 的光吸收增益 $G_{abs}$, 图中曲线展示了周期 $P$ 的变化对 Si 在同一入射波长下的光吸收增益 $G_{abs}$ 产生的影响。在入射光 $\lambda$ = 498 nm 处, 若 $P$ = 65.0 nm, 则 $G_{abs}$ 为 34%; 当 $P$ < 65.0 nm 时, $G_{abs}$ 随周期 $P$ 的增加而增加; 当 $P$ > 65.0 nm 时, $G_{abs}$ 随高度 $P$ 的增加而降低, $G_{abs}$ 总体表现出先增大后减小的变化趋势。分析认为: 周期 $P$ 增加会影响相邻颗粒偶极子的极化效果[38], 使颗粒间隙的局域电磁场强度发生变化, 当周期 $P$ = 65.0 nm 时, 局域电磁场的相互作用使金属颗粒极化率 $\alpha$ 最大, Si 的光吸收增益 $G_{abs}$ 最高; 当 $P$ < 65.0 nm 时相邻 Ag-NPs 内偶极子之间的耦合过强, 增加了 Ag-NPs 的光吸收损耗 $A_{metal}$, 导致 Si 的光吸收减少、光吸收增益 $G_{abs}$ 降低; 当 $P$ > 65.0 nm 时, 相邻 Ag 纳米颗粒内偶极子间的相互作用随周期 $P$ 的增加而降低, 尽管 Ag-NPs 的非辐射损耗效应得到抑制[38], 但由于入射场与 Ag-

NPs 的耦合效应减弱，导致 LSPs 强度因周期 $P$ 的增加而降低[38]，使反射率 $R$ 有所提高，导致 Si 的光吸收增益 $G_{abs}$ 随阵列周期 $P$ 的增加而降低。

根据上述计算结果知，当 Ag 纳米颗粒阵列的半径 $r$ = 22.5 nm、高度 $H$ = 60.0 nm 与周期 $P$ = 65.0 nm 时，Si 的光吸收率 $A_{Si}$ 最高，为 83%，吸收峰位为 $\lambda_{peak}$ = 498 nm，该峰值波长处于蓝光波段边缘。为了适应目前对蓝光 LED 的高效光探测需求，有必要继续调整优化，使 Si 对蓝光最大吸收发生在 440~480 nm 区域。

### 3.2 LSPR 效应对 Si 的光吸收增强机理

前面计算了 Ag-NPs 的各几何参数对 Si 吸收光的影响，在此基础上，经对 Ag 纳米颗粒的半径 $r$、高度 $H$、周期 $P$ 与相邻粒子间距 $D$ 的多次优化计算，最终得出：当 $r$ =18.5 nm，$H$ = 45.0 nm，$P$ = 49.0 nm 时，Ag-NPs/Si 复合结构 Si 的光吸收率最高，约为 94%，共振波长 $\lambda_{peak}$ = 465 nm，如图 6(a)所示。图中单一介质 Si 的光吸收谱源于 FDTD 算法对入射光场与 Si[25] 相互作用的计算结果。通过图中的计算结果发现，在 Ag-NPs/Si 结构中，Si 未能实现完美的蓝光吸收。根据式(5)可知，$A_{Si} = 1 - A_{metal} - R$，由于 Ag-NPs 的光能量吸收损耗 $A_{metal}$ 与反射率 $R$ 存在(根据 Si 的色散特性，Ag-NPs/Si 模型中 Si 的设计厚度远大于蓝光的透入深度，蓝光被 Si 几乎全部吸收，透射率 $T$ 可忽略)，使得波长为 $\lambda$ = 465 nm 的入射光未能被 Si 全部吸收($A_{Si}$ < 100%)，并且在 Si 的光吸收谱中也存在双吸收峰，对该现象前文已做出解释，不再赘述。将图 6(a)的计算结果代入式(7)，可得到图 6(b)Si 的光吸收增益，可见，在 $\lambda$ = 465 nm 处具有最高的光吸收增益 $G_{abs}$ = 57%。

通过探究 LSPR 效应对 Si 在蓝光波段光吸收的影响，由于 Ag 材料在蓝绿波段的吸收损耗 $A_{metal}$ 极低[26]，而由前文知透射率 $T$ = 0，因此，通过公式(5)可知：Si 的蓝光吸收增强现象源于该波段表面反射率 $R$ 的降低。当入射光频率 $\omega_{in}$ 与局域表面等离激元共振频率 $\omega_{LSPR}$ 相匹配，满足 $\mathrm{Re}[\varepsilon] = -2\varepsilon_m$ 条件下而产生的 LSPR 效应会使 Ag-NPs 具有极大的消光截面(小尺寸颗粒，以吸收截面为主)[22]，此时，入射场能量转换为颗粒内部偶极子的振荡动能，从而有效降低了 Si 表面的光反射率 $R$。然而，根据金属颗粒极化率 $\alpha$ 的定义式(1)，通过 Ag 材料复介电常数的色散关系[28]可知，若其它频率的入射波段(即 $\omega_{in} \neq \omega_{LSPR}$)作用 Ag-NPs，会引起金属介电常数 $\mathrm{Re}[\varepsilon] \neq -2\varepsilon_m$，导致极化率 $\alpha$ 较小，此时，入射光与 Ag-NPs 的耦合效应降低，使颗粒处于非共振状态，导致反射率 $R$ 在理论上再次提高。在 Si 表面上方 1 μm 处检测光反射能量，在相同计算条件下基于 FDTD 算法求得反射率 $R$，如图 7 所示。通过图 6 与图 7 对比知：当 $\lambda_{in}$ 以 465 nm 入射 Si 表面时，光的反射率 $R_1 \approx 0.41$，根据公式(5)可得 Si 的光吸收率 $A_1 \approx 0.59$(无 Ag-NPs，$A_{metal}$ = 0)；入射 Ag-NPs/Si 结构时，光反射率 $R_2 \approx 0.01$，反射率降低，根据 FDTD 数值方法计算的 Ag-NPs 的光吸收损耗 $A_{metal} \approx 0.05$，如图 8所示。图中曲线展示了 Ag-NPs 的理论蓝光吸收损耗，其与 M.A García[34] 计算的直径为 40 nm 的 Ag-NPs 的光吸收损耗类似(文献 [34] 中图 8 所示)，将本文的 Ag-NPs 的光吸收损耗 $A_{metal}$ 代入式(5)得到基于 Ag-NPs 阵列 Si 的光吸收率 $A_2 \approx 0.94$，与 $A_1 \approx 0.59$ 相比，Si 的光吸收增强。通过图 8的曲线还发现，尽管入射波长 $\lambda_{in}$ > 465 nm 时 Ag-NPs 的光吸收损耗 $A_{metal}$ 小于 0.05，但由图 7 的反射曲线可知，反射率 $R$ 在逐渐提高，基于公式(5)计算得到的 Si 的光吸收 $A_{Si}$ < 0.94。例如在 $\lambda$ = 475 nm 处，$R$ = 0.04，$A_{metal}$ = 0.03 时，代入式(5)得$A_{Si} \approx 0.93$。

由上述数据可知，LSPR 效应使 Si 表面的反射率降低，绝大多数入射光能量被 Ag-NPs 耦合至 Si 内部。

### 3.3 Ag-NPs 阵列对光生载流子的增益

载流子生成数量对半导体光电探测器的量子效率有一定影响。若用电子—空穴对生成率 $G_e(x)$ 表征光生载流子数量[41]：

$$G_e(x) = \Phi_0 \alpha \exp(-\alpha x) = \frac{(1-R)P_{opt}}{S \cdot h\upsilon} \alpha \exp(-\alpha x), \tag{10}$$

式中，$\Phi_0$ 表示入射光子通量，$R$ 为反射率，$P_{opt}$ 为入射光功率(W/m$^2$)，$S$ 为入射面积(m$^2$)，$h\upsilon$ 为单光子能量(eV)，$\alpha$ 为介质的吸收系数(m$^{-1}$)。入射光功率密度为 1 W/m$^2$，可看作硅的光吸收能量(无向空气传播的内能损耗)全部换为空穴-电子

对, 计算条件与 2.2 节相同。利用 FDTD 算法与式(10)计算在 $\lambda_{in}=465$ nm 时, 半径 $r=18.5$ nm、高度 $H=45.0$ nm、周期 $P=49.0$ nm 的 Ag-NPs 阵列下 Si 的初始光生载流子数量, 结果如图 9(a)所示, 其中, 曲线横轴表示入射光在 Si 内部的传播距离。图中载流子数量对比曲线说明 LSPR 效应可提高 Si 的光生载流子数量, 这间接表明在硅内部更深处会产生一定数量的光生载流子。

设 $G$ 为光生载流子数量($m^{-3}$), $M$ 为光生载流子数量增益比:

$$M=\frac{G_{\text{Ag-NPs/Si}}-G_{\text{Si}}}{G_{\text{Si}}}, \tag{11}$$

式中, $G_{\text{Ag-NPs/Si}}$ 与 $G_{\text{Si}}$ 分别为基于 Ag-NPs 阵列 Si 与单一介质 Si 的光生载流子浓度, 将图 9(a)中计算的载流子数量代入式(11)可得到基于 Ag-NPs 阵列 Si 的光生载流子数量增益 $M\approx0.53$, 结果如图 9(b)所示。由式(10)定义的 $G_e(x)$ 可知: 光生载流子数量的增益与 Ag-NPs/Si 结构的反射率 $R$ 降低有关。变化物理机制在前文已做说明, 在此不做赘述。由此可得出以下结论: 在理论上 LSPR 效应可提高光生载流子数量, 增加载流子被电极收集的概率, 增强 Si 基光电探测器的量子效率。

## 4　结　论

本文研究了 Ag-NPs/Si 复合结构对可见光吸收的影响。在蓝光波段下, 分别计算了 Ag-NPs 的几何参数半径 $r$、高度 $H$ 和周期 $P$ 与 Si 的光吸收的关系。得到以下结论: 当半径 $r$ 增加时, Si 的光吸收率增大, 共振峰位红移; 当高度 $H$ 增加时, Si 的光吸收率先增大后减小, 共振峰位红移; 当周期 $P$ 增加时, Si 的光吸收率先增大后减小, 共振峰位蓝移。对 Ag-NPs/Si 复合结构的优化结果表明: 在 Ag-NPs 结构中, $r=18.5$ nm, $H=45.0$ nm, 周期 $P=49.0$ nm 时, Si 的最高吸收率为 94%, 最大吸收峰值波长 $\lambda=465$ nm, 光吸收增益为 0.57; 计算 Ag-NPs/Si 在 $\lambda=465$ nm 处的光生载流子数量增益约为 0.53。硅的光吸收增强及光生载流子数量提高与由 LSPR 效应引起的 Si 表面反射率降低有关。本文研究结果对设计基于 Ag-NPs 增强蓝光探测响应度的硅基可见光光电探测器具有良好的参考价值。

**参考文献:**


[1] 秦沛, 任玉, 刘丽炜, 等. 金属纳米颗粒等离激元共振增强非线性介质谐波的发展现状[J]. 中国光学, 2016, 9(2): 213-225.
QIN P, REN Y, LIU L W, *et al*.. Development of plasmon-resonance of metal nanoparticles enhanced harmonic generation in nonlinear medium[J]. *Chinese Optics*, 2016, 9(2): 213-225. (in Chinese)

[2] 雷建国, 刘天航, 林景全, 等. 表面等离子体激元的若干新应用[J]. 中国光学, 2010, 3(5): 432-439.
LEI J G, LIU T H, LIN J Q, *et al*.. New applications of surface plasmon polaritons[J]. *Chinese Optics*, 2010, 3(5): 432-439. (in Chinese)

[3] MA G H, ZHANG J B, ZHANG H, *et al*.. Resonant mode of Fabry-Perot microcavity regulated by metal surface plasmons[J]. *Chinese Optics*, 2019, 12(3): 649-662.

[4] 相春平, 袁占生, 刘璟, 等. 表面等离子激元与F-P共振耦合平衡钙钛矿太阳能电池有源层内载流子产生速率[J]. 发光学报, 2018, 39(12): 1749-1756.
XIANG CH P, YUAN ZH SH, LIU J, *et al*.. Surface plasmon polaritons and F-P resonance coupled modes balance the generation rate of charge carriers of Perovskite solar cells[J]. *Chinese Journal of Luminescence*, 2018, 39(12): 1749-1756. (in Chinese)

[5] 许恒, 闫龙, 李玲, 等. 局域表面等离激元对InGaN/GaN多量子阱发光效率的影响[J]. 发光学报, 2017, 38(3): 324-330.
XU H, YAN L, LI L, *et al*.. Influence of localized surface Plasmons on the photoluminescence efficiency of InGaN/GaN multiple quantum wells[J]. *Chinese Journal of Luminescence*, 2017, 38(3): 324-330. (in Chinese)

[6] 乔倩, 单崇新, 刘娟意, 等. 不同密度银纳米粒子对氧化锌基发光二极管发光的增强[J]. 发光学报, 2015, 36(12):

1363-1369.
QIAO Q, SHAN CH X, LIU J Y, *et al*.. Localized surface plasmon resonance enhanced electroluminescence from ZnO-based light-emitting diodes *via* optimizing the density of sliver nanoparticles[J]. *Chinese Journal of Luminescence*, 2015, 36(12): 1363-1369. (in Chinese)

[7] BUTUN S, CINEL N A, OZBAY R. Nanoantenna coupled UV subwavelength photodetectors based on GaN[J]. *Optics Express*, 2012, 20(3): 2649-2656.

[8] 乔静, 谢生, 毛陆虹, 等. 吸收增强的光栅型金属-半导体-金属光电探测器的优化设计[J]. 发光学报, 2018, 39(3): 363-368.
QIAO J, XIE SH, MAO L H, *et al*.. Optimum design of silicon-based metal-semiconductor-metal photodetector with subwavelength metal grating[J]. *Chinese Journal of Luminescence*, 2018, 39(3): 363-368. (in Chinese)

[9] 邵伟佳. 基于表面等离子体激元的光学滤波片与完美吸收超材料的设计及数值模拟[D]. 合肥: 中国科学技术大学, 2014.
SHAO W J. Design and numerical simulation of optical filter and metamaterial perfect absorber based on surface plasmon polaritons[D]. Hefei: University of Science and Technology of China, 2014. (in Chinese).

[10] WOKAUN A, GORDON J P, LIAO P F. Radiation damping in surface-enhanced raman scattering[J]. *Physical Review Letters*, 1982, 48(14): 957-960.

[11] CLAVERO C. Plasmon-induced hot-electron generation at nanoparticle/metal-oxide interfaces for photovoltaic and photocatalytic devices[J]. *Nature Photonics*, 2014, 8(2): 95-103.

[12] KNIGHT M W, SOBHANI H, NORDLANDER P, *et al*.. Photodetection with active optical antennas[J]. *Science*, 2011, 332(6030): 702-704.

[13] LI D B, SUN X J, SONG H, *et al*.. Realization of a high-performance GaN UV detector by nanoplasmonic enhancement[J]. *Advanced Materials*, 2012, 24(6): 845-849.

[14] SOBHANI A, KNIGHT M W, WANG Y M, *et al*.. Narrowband photodetection in the near-infrared with a plasmon-induced hot electron device[J]. *Nature Communications*, 2013, 4(1): 1643.

[15] BAO G H, LI D B, SUN X J, *et al*.. Enhanced spectral response of an AlGaN-based solar-blind ultraviolet photodetector with Al nanoparticles[J]. *Optics Express*, 2014, 22(20): 24286-24293.

[16] QU D, LIU F, YU J F, *et al*.. Plasmonic core-shell gold nanoparticle enhanced optical absorption in photovoltaic devices[J]. *Applied Physics Letters*, 2011, 98(11): 113119.

[17] 刘洋, 蔡喜平, 林朗, 等. LED可见光通信网络与以太网互融技术的研究[J]. 光通信技术, 2019, 43(1): 1-4.
LIU Y, CAI X P, LIN L, *et al*.. Research on the fusion technology of LED visible optical communication network with ethernet[J]. *Optical Communication Technology*, 2019, 43(1): 1-4. (in Chinese)

[18] 迟楠, 王超凡, 李韦萍, 等. 基于蓝绿光LED的水下可见光通信技术研究进展[J]. 复旦学报 (自然科学版), 2019, 58(5): 537-548.
CHI N, WANG CH F, LI W P, *et al*.. Research progress of underwater visible light communication technology based on blue/green LED[J]. *Journal of Fudan University* (*Natural Science*), 2019, 58(5): 537-548. (in Chinese)

[19] 赵太飞, 马壮, 李星善, 等. 近距离LED光通信直视信道模型研究[J]. 光子学报, 2020, 49(1): 106001.
ZHAO T F, MA ZH, LI X SH, *et al*.. Research on line-of-sight channel model of short-range LED optical communication[J]. *Acta Photonica Sinica*, 2020, 49(1): 106001. (in Chinese)

[20] TAFLOVE A, HAGNESS S C. *Computational Electrodynamics*: *The Finite-Difference Time-Domain Method*[M]. 2nd ed. Boston: Artech House, 2000.

[21] 朱旭鹏, 张轼, 石惠民, 等. 金属表面等离激元耦合理论研究进展[J]. 物理学报, 2019, 68(24): 247301.
ZHU X P, ZHANG SH, SHI H M, *et al*.. Research progress of coupling theory of metal surface plasmon[J]. *Acta Physica Sinica*, 2019, 68(24): 247301. (in Chinese)

[22] 丛超. 贵金属纳米颗粒的局域表面等离激元共振特性研究[D]. 南京: 南京大学, 2011.
CONG CH. Localized surface plasmon resonance properties of noble metal nanoparticles[D]. Nanjing: Nanjing University, 2011. (in Chinese).

[23] BAI Y C, GAO C B, YIN Y D. Fully alloyed Ag/Au nanorods with tunable surface plasmon resonance and high

chemical stability[J]. *Nanoscale*, 2017, 9(39): 14875-14880.

[24] WEST P R, ISHII S, NAIK G V, *et al*.. Searching for better plasmonic materials[J]. *Laser & Photonics Reviews*, 2010, 4(6): 795-808.

[25] SCHINKE C, PEEST P C, SCHMIDT J, *et al*.. Uncertainty analysis for the coefficient of band-to-band absorption of crystalline silicon[J]. *AIP Advances*, 2015, 5(6): 067168.

[26] PALIK E D. *Handbook of Optical Constants of Solids*[M]. New York: Academic Press, 1998.

[27] 王善江, 苏丹, 张彤. 表面等离激元光热效应研究进展[J]. 物理学报, 2019, 68(14): 144401.
WANG SH J, SU D, ZHANG T. Research progress of surface plasmons mediated photothermal effects[J]. *Acta Physica Sinica*, 2019, 68(14): 144401. (in Chinese)

[28] MIE G J A P. Articles on the optical characteristics of turbid tubes, especially colloidal metal solutions[J]. *Annals of Physics*, 1908, 25(3): 377-445.

[29] KELLY K L, CORONADO E, ZHAO L L, *et al*.. The optical properties of metal nanoparticles: the influence of size, shape, and dielectric environment[J]. *The Journal of Physical Chemistry B*, 2003, 107(3): 668-677.

[30] PIETROBON B, MCEACHRAN M, KITAEV V. Synthesis of size-controlled faceted pentagonal silver nanorods with tunable plasmonic properties and self-assembly of these nanorods[J]. *ACS Nano*, 2009, 3(1): 21-26.

[31] LINK S, EL-SAYED M A. spectral properties and relaxation dynamics of surface plasmon electronic oscillations in gold and silver nanodots and nanorods[J]. *The Journal of Physical Chemistry B*, 1999, 103(40): 8410-8426.

[32] KHLEBTSOV B, KHANADEEV V, KHLEBTSOV N. Tunable depolarized light scattering from gold and gold/silver nanorods[J]. *Physical Chemistry Chemical Physics*, 2010, 12(13): 3210-3218.

[33] MAILLARD M, GIORGIO S, PILENI M P. Tuning the size of silver nanodisks with similar aspect ratios: synthesis and optical properties[J]. *The Journal of Physical Chemistry B*, 2003, 107(11): 2466-2470.

[34] GARCIA M A. Surface plasmons in metallic nanoparticles: fundamentals and applications[J]. *Journal of Physics D*: *Applied Physics*, 2011, 44(28): 283001.

[35] 赖淑妹, 黄志伟, 王仰江, 等. Ag纳米结构局域表面等离激元共振模拟与分析[J]. 激光与光电子学进展, 2018, 55(12): 122601.
LAI SH M, HUANG ZH W, WANG Y J, *et al*.. Simulation and analysis of local surface plasmon resonance of Ag nanostructures[J]. *Laser & Optoelectronics Progress*, 2018, 55(12): 122601. (in Chinese)

[36] LINK S, El-SAYED M A. Size and temperature dependence of the plasmon absorption of colloidal gold nanoparticles[J]. *The Journal of Physical Chemistry B*, 1999, 103(21): 4212-4217.

[37] LINK S, MOHAMED M B, EL-SAYED M A. Simulation of the optical absorption spectra of gold nanorods as a function of their aspect ratio and the effect of the medium dielectric constant[J]. *The Journal of Physical Chemistry B*, 1999, 103(16): 3073-3077.

[38] MARKEL V A. Coupled-dipole approach to scattering of light from a one-dimensional periodic dipole structure[J]. *Journal of Modern Optics*, 1993, 40(11): 2281-2291.

[39] ZOU SH L, JANEL N, SCHATZ G C. Silver nanoparticle array structures that produce remarkably narrow plasmon lineshapes[J]. *The Journal of Chemical Physics*, 2004, 120(23): 10871-10875.

[40] ROCKSTUHL C, FAHR S, LEDERER F. Absorption enhancement in solar cells by localized plasmon polaritons[J]. *Journal of Applied Physics*, 2008, 104(12): 123102.

[41] GÄRTNER W W. Depletion-layer Photoeffects in semiconductors[J]. *Physical Review*, 1959, 116(1): 84-87.

Author Biographics:

Wang Haobing (1994—), male, born in Songyuan City, Jilin province, Master Degree Candidate. In 2017, he graduated from Changchun University of Science and Technology with a Bachelor of Science degree. He is now a graduate student of Changchun Institute of Optics, Fine Mechanics and Physics, Chinese Academy of Sciences. He is mainly engaged in the research of nanophotonics and semiconductor photodetectors. E-mail: 996490955@qq.com

王浩冰(1994—),男,吉林松原人,硕士研究生,2017 年于长春理工大学获得理学学士学位,主要从事纳米光子学与半导体光电探测器方面的研究。E-mail: 996490955@qq.com

Liang Jingqiu (1962—), female, born in Changchun City, Jilin Province. She is a doctor, researcher and doctoral supervisor. In 2003, she received her doctor's degree from Changchun Institute of Optics, Fine Mechanics and Physics, Chinese Academy of Sciences. Now she is a researcher of this institute. She is mainly engaged in the research of micro/nano optical structures, devices and systems, infrared spectrum/imaging spectrum and infrared optical instruments, micro LED microdisplay chip and its application, and visible light communication devices and systems. E-mail: liangjq@ciomp.ac.cn

梁静秋(1962—),女,吉林长春人,博士,研究员,博士生导师,2003 年于中国科学院长春光学精密机械与物理研究所获得博士学位,主要从事微/纳光学结构、器件与系统研究、红外光谱/成像光谱技术及红外光学仪器研究、micro LED 微显示芯片及应用研究与可见光通信器件及系统方面的研究。E-mail: liangjq@ciomp.ac.cn

Wang Weibiao (1962—), male, born in Yangzhou City, Jiangsu province. He is a doctor, researcher and doctoral supervisor. He received his doctor 's degree from Changchun Institute of Optics, Fine Mechanics and Physics, Chinese Academy of Sciences in 1999. Now he is a researcher of this institute. He is mainly engaged in the research of photonic crystal and micro-nano photonics, LED array chip integration and application, field emission materials and electron emission characteristics. E-mail: wangwb@ciomp.ac.cn

王惟彪(1962—),男,江苏扬州人,博士,研究员,博士生导师,1999 年于中国科学院长春光学精密机械与物理所获得博士学位,现为中国科学院长春光学精密机械与物理研究所研究员。主要从事光子晶体及微纳光子学研究、发光二极管(LED)阵列芯片集成及应用研究、场发射材料与电子发射特性方面的研究。E-mail: wangwb@ciomp.ac.cn